Title

Pain modulates dopamine neurons via a spinal–parabrachial–mesencephalic circuit

Journal

Nature Neuroscience, 24(10)

ISSN

1097-6256

Authors

Yang, Hongbin
de Jong, Johannes W
Cerniauskas, Ignas
et al.

Publication Date

2021-10-01

DOI

10.1038/s41593-021-00903-8

Peer reviewed

HHS Public Access

Author manuscript

Nat Neurosci. Author manuscript; available in PMC 2022 October 01.

Published in final edited form as:

Nat Neurosci. 2021 October ; 24(10): 1402–1413. doi:10.1038/s41593-021-00903-8.

Pain modulates dopamine neurons via a spino-parabrachio-mesencephalic circuit

Hongbin Yang[1,#], **Johannes W. de Jong**[1], **Ignas Cerniauskas**[1], **James R. Peck**[1], **Byung Kook Lim**[2], **Hui Gong**[3,4], **Howard L. Fields**[5], **Stephan Lammel**[1,6,*]

[1]Department of Molecular and Cell Biology and Helen Wills Neuroscience Institute, University of California Berkeley, Berkeley, CA 94720, USA

[2]Neurobiology Section, Division of Biological Sciences, University of California, San Diego, La Jolla, CA 92037, USA

[3]Britton Chance Center for Biomedical Photonics, Wuhan National Laboratory for Optoelectronics, MoE Key Laboratory for Biomedical Photonics, School of Engineering Sciences, Huazhong University of Science and Technology, Wuhan, China

[4]HUST-Suzhou Institute for Brainsmatics, JITRI Institute for Brainsmatics, Suzhou, China

[5]Alcohol and Addiction Research Group, Department of Neurology, University of California, San Francisco, San Francisco, CA 94158, USA

[6]Lead Contact

Abstract

Pain decreases the activity of many ventral tegmental area (VTA) dopamine (DA) neurons, yet the underlying neural circuitry connecting nociception and the DA system is not understood. Here we show that a subpopulation of lateral parabrachial (LPB) neurons is critical for relaying nociceptive signals from the spinal cord to the substantia nigra pars reticulata (SNR). SNR-projecting LPB neurons are activated by noxious stimuli and silencing them blocks pain responses in two different models of pain. LPB-targeted and nociception-recipient SNR neurons regulate VTA DA activity directly through feedforward inhibition and indirectly by inhibiting a distinct subpopulation of VTA-projecting LPB neurons thereby reducing excitatory drive onto VTA DA neurons. Correspondingly, ablation of SNR-projecting LPB neurons is sufficient to reduce pain-mediated inhibition of DA release *in vivo*. The identification of a neural circuit conveying nociceptive input to DA neurons is critical to our understanding of how pain influences learning and behavior.

[*]Correspondence to: Stephan Lammel, Ph.D. Department of Molecular and Cell Biology and Helen Wills Neuroscience Institute 142 Life Science Addition #3200 University of California Berkeley Berkeley, CA 94720, USA, Phone: 510 664 7821, lammel@berkeley.edu.

[#]present address: MOE Frontier Science Center for Brain Research and Brain-Machine Integration, Zhejiang University Medical Center; School of Brain Science and Brain Medicine, Zhejiang University, Hangzhou 310058, China

AUTHOR CONTRIBUTIONS

Stereotactic injections were performed by H.Y. Immunohistochemistry was performed by H.Y. and J.R.P. *Ex vivo* electrophysiology was performed by H.Y. *In vivo* electrophysiology was performed by J.W.J, I. C. and H.Y. Fiber photometry was performed by J.W.J. Critical viral reagents B.K.L. fMOST was performed by H.G. Behavior experiments and optogenetics were performed by H.Y. and J.W.J. The study was designed by H.Y., H.F. and S.L. Results were analyzed and interpreted by H.Y., J.W.J., H.F. and S.L. The manuscript was written by H.Y. and S.L. and edited by all authors.

COMPETING INTERESTS STATEMENT

The authors declare no competing interests.

INTRODUCTION

Dopamine (DA) neurons in the ventral tegmental area (VTA) are critical in reward and motivation[1–4], but their crucial role in behavioral responses to pain is less clear[5–8]. Many VTA DA neurons reduce their activity in response to acute painful stimuli[9–13], whereas pain relief increases DA levels in the brain[6,10,14]. Chronic pain is common in hypodopaminergic conditions such as Parkinson's disease[15], and DA dysfunction has been associated with neuropathic pain[16–18], which could be related to several of the comorbid symptoms such as reduced motivation and depression[18,19]. Thus, while animal and human studies provide evidence that acute and chronic pain affect VTA DA neurons, which may modulate the affective motivational aspects of pain[6], the neural circuit that transmits nociceptive signals from the periphery to DA neurons is not well understood.

One major ascending nociceptive pathway from the spinal cord dorsal horn terminates in the lateral parabrachial nucleus (LPB)[20–22]. Electrophysiological recordings in anesthetized rats and calcium imaging studies in awake behaving mice have shown that LPB neurons respond to a wide range of noxious stimuli[9,22–24]. From the LPB, nociceptive information is distributed to key areas of the brain that trigger emotions and fear (amygdala, periaqueductal grey), pain sensation (intralaminar thalamic nucleus) and autonomic homeostatic adaptation (hypothalamus and ventrolateral medulla)[21,25–28]. LPB neurons also project to the VTA[29] and nociceptive responsive LPB neurons may be a critical link in the transmission of pain-related information to VTA DA neurons[9].

RESULTS

Two anatomically distinct LPB pathways to VTA and SNR

To examine the anatomical organization of LPB projections, we combined anterograde adeno-associated virus (AAV) tracing of LPB neurons and fluorescent micro-optical sectioning tomography (fMOST) with whole-brain imaging in adult mice (Fig. 1a and Supplementary Movie 1). Consistent with previous studies[9,28,29], analysis of eYFP-expressing glutamatergic LPB (LPB_{VGLUT2}) projections revealed dense innervations of numerous forebrain regions including the bed nucleus of the stria terminalis (BNST), thalamus, lateral hypothalamus (LH), central nucleus of the amygdala (CeA), and ventral midbrain, in particular lateral substantia nigra pars reticulata (SNR) and VTA (Extended Data Fig. 1a–h). Our high-resolution whole-brain dataset allowed us to determine that the ventral midbrain contains both fibers of passage and terminals (Fig. 1b,c). eYFP-expressing fibers of passage were most prominent in the medial VTA, whereas eYFP-expressing terminals were abundant in both the lateral VTA and SNR (Extended Data Fig. 1f,g and Supplementary Movie 2). Consistent with this, synaptophysin-expressing LPB_{VGLUT2} terminals were located in the lateral VTA and SNR but to a lesser extent in the medial VTA (Extended Data Fig. 1i–k). Conversely, whole brain mapping of projections of GABAergic LPB (LBP_{GAD2}) neurons revealed eYFP-expressing terminals in the dorsolateral periaqueductal gray (PAG) but not in the ventral midbrain or amygdala (Extended Data Fig. 1p–s).

Next, we performed retrograde tracing of the SNR, VTA and CeA and found that LPB neurons projecting to these structures are anatomically segregated. SNR-projecting LPB neurons (LPB→SNR) were mainly located in the dorsal LPB (LPBd), whereas VTA-projecting LPB neurons (LPB→VTA) were found in the central LPB (LPBc). CeA-projecting LPB neurons were located in the external LPB (Fig. 1d–f)[27]. To further examine whether VTA- and SNR-projecting LPB neurons are part of separate circuits, we used a rabies virus-based tracing strategy[10] to map whole-brain monosynaptic inputs onto the two cell populations (Extended Data Fig. 2a). Histological analysis revealed the localization of starter cells (i.e., cells that are both TVA-mCherry- and RV-GFP-immunopositive) in the LPB (Extended Data Fig. 2b–e). We then determined the anatomical locations and number of GFP-expressing cells that synapse onto VTA- and SNR-projecting LPB neurons. We found that while they receive qualitatively similar inputs, VTA-projecting LPB neurons receive a significantly greater share of input from the laterodorsal tegmentum (LDT), dorsal raphe nucleus (DR), periaqueductal gray (PAG) and SNR (Extended Data Fig. 2f,g).

Next, we examined whether LPB neurons make functional synaptic connections onto VTA and SNR cell populations (Fig. 1g). The VTA contains heterogenous cell populations including dopaminergic, GABAergic and glutamatergic neurons[30]. Importantly, VTA DA subpopulations have distinct anatomical, molecular, and functional properties[10,31]. The lateral VTA predominantly contains DA neurons projecting to NAc lateral shell (NAcLat)[10,31]. Based on the abundance of LBP_{VGLUT2} terminals in the lateral VTA (Extended Data Fig. 1f, i–k), it is possible that DA neurons projecting to NAcLat receive pain-related information directly from the LPB, although it seems unlikely given that we previously demonstrated that DA neurons projecting to NAcLat show robust inhibitory responses following noxious or aversive stimuli[10]. On the other hand, LPB_{VGLUT2} neurons might target VTA DA neurons indirectly by activating VTA GABA neurons, which exert strong inhibitory influence over VTA DA neurons including those projecting to NAcLat[31]. Hence, we examined functional synaptic connectivity between LPB_{VGLUT2} neurons and VTA DA neurons projecting to NAcLat VTA GABA neurons as well as cells in the SNR, as the latter structure appears to be innervated by an anatomically distinct LPB cell population. Unexpectedly, light stimulation of channelrhodopsin-2 (ChR2)-expressing LPB_{VGLUT2} terminals produced large excitatory postsynaptic currents (EPSCs) in all NAcLat-projecting VTA DA neurons (n = 21/21 cells; tyrosine hydroxylase (TH)-immunopositive) and all SNR neurons (n = 25/25 cells; TH-immunonegative), whereas only 2 out 10 VTA GABA ($VTA_{GAD2tdT+}$) cells showed very small EPSCs following stimulation of LPB_{VGLUT2} inputs (Fig. 1h,i,k and Extended Data Fig. 1t–v). Light-evoked EPSCs were blocked by co-application of AMPA (α-amino-3-hydroxy-5-methyl-4-isoxazole propionic acid) and NMDA (N-methyl-D-aspartate) receptor antagonists (CNQX and APV, respectively) indicating that LPB terminals released glutamate (Fig. 1j). SNR neurons that receive excitatory input from the LPB express VGAT, suggesting that they are GABAergic (Extended Data Fig. 1l–o). Notably, NAcLat-projecting DA neurons and SNR cells, both recorded in the same set of slices, significantly increased firing in response to 10 Hz light stimulation of LPB_{VGLUT2} inputs (Fig. 1l,m).

Our results reveal two non-overlapping, previously uncharacterized excitatory LPB pathways to lateral VTA DA neurons and SNR GABA neurons. The unexpected conundrum

that the LPB, a structure that is known to relay noxious sensory stimuli, directly excites NAcLat-projecting VTA DA neurons which, conversely, are inhibited by aversive or noxious stimuli[16] led us to further dissect the anatomy and functional role of the two LPB pathways for nociception.

Spinal cord, dorsal horn neurons target LPB→SNR neurons

The LPB is a target for ascending projections from nociceptive-responsive neurons in the spinal cord dorsal horn[20,22,25]. To investigate whether LPB→VTA and LPB→SNR neurons receive direct synaptic input from the spinal cord, we injected an AAV expressing ChR2-eYFP into the dorsal horn of the spinal cord (L4-L5) and a retrogradely-transported canine adenovirus expressing Cre-recombinase (CAV2-Cre) to the SNR or lateral VTA of tdTomato (tdT) reporter mice (Fig. 2a). ChR2-eYFP-expressing terminals were located in the LPBd in close proximity to SNR-projecting (i.e., $CAV2_{tdT+}$) LPB neurons and to a lesser extent in the LPBc, which contained most of the VTA-projecting (i.e., $CAV2_{tdT+}$) LPB neurons (Fig. 2b,c). Patch-clamp recordings confirmed light-evoked EPSCs (blocked by CNQX) in 42% of the recorded LPB→SNR cells (n = 14/33 cells), but only in 16% of LPB→VTA neurons (n = 5/32 cells; Fig. 2d). Thus, ascending nociception-specific neurons in the dorsal horn preferentially target LPB→SNR neurons.

LPB→SNR neurons are excited by noxious stimuli

Because a large proportion of LPB→SNR neurons receive input from the dorsal horn, we hypothesized that LPB→SNR neurons are activated by acute noxious stimuli. To test our hypothesis, we utilized fiber photometry to measure calcium dynamics from LPB→SNR neurons in response to diverse noxious and innocuous stimuli (electrical shock, tail brush, tail pinch, heat; n = 5 mice; Fig. 3a and Supplementary Fig. 1a). We observed large increases in calcium activity that were time-locked to the delivery of electrical tail shock (Fig. 3b,c) or tail pinch (Fig. 3e,f), whereas tail brush had a much weaker, if any, effect (Fig. 3d). Exposing a mouse tail to hot water significantly increased calcium transients when temperatures increased from 40°C to 50°C and 55°C (Fig. 3g,h).

Fiber photometry does not provide information about the activity of individual neurons. Indeed, when we performed *in vivo* tetrode recordings from (non-projection defined) LPB neurons, we also found a smaller, though appreciable, number of cells that were inhibited by noxious stimuli (Extended Data Fig. 3). This finding led us to examine how individual (projection-defined) LPB→SNR cells respond to noxious stimuli. We tagged these cells with ChR2 by injecting retrogradely-transported AAV expressing Cre recombinase (AAVretro-Cre) into the SNR and AAV carrying Cre-dependent ChR2-mCherry (AAV-DIO-ChR2-mCherry) into the LPB of C57BL/6 mice (n = 6 mice). A driveable optoelectrode (optrode) was implanted above the LPB and lowered ~40 μm after each recording session (Fig. 3i). Cre-mediated ChR2-mCherry expression and optrode placement in the LPB was confirmed using histology (Fig. 3j and Supplementary Fig. 1b). To identify LPB neurons that expressed ChR2 (i.e., LPB→SNR neurons), we tested whether recorded LPB cells responded with minimal latency to 473 nm light stimulation. Consistent with direct excitation (Supplementary Fig. 1c–g), all optogenetically-identified LPB neurons responded with short latency (4.57 ± 0.49 ms, n = 17 cells) after the light onset (Fig. 3k). Comparison

of spontaneous and light-evoked spikes revealed that stimulation did not produce detectable changes in the action potential shape (Fig. 3l). After ChR2-tagged LPB→SNR neurons were identified, two different noxious stimuli (heat and electrical shock) were administered to the animals. Although the majority of LPB→SNR neurons were excited by these stimuli, we also found some cells that were inhibited (Fig. 3m–p).

The differences between population- and single cell-level analysis led us to perform additional experiments to further investigate the responsiveness of LPB→SNR neurons to noxious stimuli: first, we found that animals exposed to noxious heat (55°C) showed a significantly increased proportion of LPB→SNR neurons that express the activity-dependent early gene *Fos* when compared to animals exposed to non-noxious heat (37°C; Extended Data Fig. 4a–c,e,f). Second, intraplantar injection of 1% formalin, a noxious chemical that induces inflammatory pain[32], significantly increased *Fos* expression in LPB→SNR neurons compared to saline-injected animals (Extended Data Fig. 4a,b,d,g,h). Third, assessment of miniature EPSCs (mEPSCs) and miniature inhibitory postsynaptic currents (mIPSCs) from LPB→SNR neurons showed that formalin-induced pain strongly affected both excitatory and inhibitory synaptic transmission (Extended Data Fig. 4i–n).

Taken together, although some LPB→SNR neurons are inhibited by noxious stimuli, a large proportion of these cells is excited.

Silencing of the LPB→SNR pathway reduces pain

To further investigate a potential role of the LPB→SNR pathway underlying pain, we optogenetically silenced LPB→SNR neurons in widely used mouse models of inflammatory and neuropathic pain[32]. We injected VGLUT2-Cre mice with AAV carrying the inhibitory opsin halorhodopsin (AAV-DIO-NpHR) or a control vector (AAV-DIO-eYFP) into the LPB and implanted optical fibers bilaterally above the SNR (Fig. 4a,b and Extended Data Fig. 5a,b). Since the SNR is a major basal ganglia output structure involved in motor control[33,34], we first examined the effects of optogenetically silencing LPB_{VGLUT2} terminals in the SNR in the open field test, but did not observe any effects on general locomotor activity (Extended Data Fig. 5c–f). Next, NpHR and eYFP mice received unilateral intraplantar injection of 1% formalin, which produced biphasic paw-licking behavior with a short initial response (phase I) and a later response (phase II)[35]. We measured the animals' licking response while exposing LPB_{VGLUT2} terminals in the SNR to 589 nm light. NpHR mice, when compared to eYFP mice, showed reduced pain-related licking behavior in phase II of the test, while no significant difference between the two groups was detected in phase I (Fig. 4c,d).

It is possible that silencing LPB inputs to the SNR is sufficient to perturb licking behavior per se, since SNR projections to superior colliculus (SC) have been shown to be involved in general licking behavior[36]. However, optogenetic silencing of the LPB→SNR pathway did not affect overall licking behavior of a 1% sucrose solution (Extended Data Fig. 5g,h), suggesting that inhibition of this pathway during the formalin test affects licking as an expression of pain instead of a motor action.

We also used the von Frey test[32] to assess the mechanical threshold for paw withdrawal responses before and after formalin injection as well as with or without light stimulation of LPB_{VGLUT2} inputs in both groups. We observed that before formalin injection, opto-silencing of LPB_{VGLUT2} terminals in the SNR did not alter withdrawal reflexes. After formalin injection, NpHR and eYFP mice showed mechanical hypersensitivity (i.e., mechanical allodynia), but only in NpHR mice did yellow light exposure dramatically increase withdrawal threshold to mechanical stimulation (Fig. 4e,f).

Additional cohorts of NpHR and eYFP mice were subjected to neuropathic pain induced by ligation of the sciatic nerve (SNL) and compared to sham (Fig. 4g). As expected, we observed mechanical and thermal hypersensitivity during von Frey and hot plate tests in the SNL, but not in the sham-operated side in both NpHR- and eYFP-expressing mice. When we exposed LPB_{VGLUT2} terminals in the SNR to yellow light, however, mechanical and thermal hypersensitivity was alleviated only in NpHR-expressing SNL mice, but had no effect in the other groups (Fig. 4h–j).

Previous studies used classic conditioning paradigms to demonstrate that animals approach contextual cues previously associated with pain relief[14,37]. To examine whether optogenetic silencing of LPB_{VGLUT2} terminals in SNR produces pain relief, we subjected NpHR- and eYFP-expressing SNL mice to a conditioning procedure in which 589 nm light was paired with only one side of a place preference box. After conditioning, when placed in the same box but without light stimulation, NpHR-expressing SNL mice increased the time that they spent in the chamber paired with light stimulation, whereas eYFP-expressing SNL mice avoided this chamber. No conditioned place preference was observed in NpHR sham-operated animals (Fig. 4k–m).

Finally, to confirm that the observed behavioral effects are specific and not caused by confounding factors that can accompany optogenetic manipulations (e.g., light-induced tissue heating, paradoxical excitation of inhibitory opsins[38]), we performed a complementary loss-of-function experiment. We induced apoptosis in SNR-projecting LPB neurons by injecting retrogradely-transported pseudotyped equine infectious anemia virus expressing Cre-recombinase (RG-EIAV-Cre) into the right SNR and AAV carrying Cre-dependent Caspase 3[39] into the right LPB of C57BL/6 mice. Control animals received injections of AAV carrying Cre-dependent eYFP instead of Caspase 3 into the right LPB, while all other procedures were identical. We first examined general locomotor activity, which did not differ between Caspase 3 and eYFP mice (Extended Data Fig. 6a–c). Animals were then injected with formalin into both hind paws and licking behavior was measured. We observed a pronounced reduction in pain-related licking during phase II in the contralateral hind paw compared to the ipsilateral hind paw, whereas pain-related licking behavior in the two hind paws was similar during phase I of the test and during both phases in eYFP animals (Extended Data Fig. 6d–h). Interestingly, while optogenetic inhibition of LPB→SNR significantly reduced lick duration but not number of licks (Fig. 4c,d), genetic ablation significantly reduced both parameters, which may be caused by different experimental conditions (e.g., more penetrant inhibition with Caspase 3 compared to eNpHR, unilateral versus bilateral formalin injections).

Altogether, we demonstrate that silencing the LPB→SNR pathway mitigates formalin- and SNL-induced nociceptive behaviors and produces pain relief associated with contextual cues.

Direct and indirect inhibition of VTA DA neurons via SNR

Next, we recorded single-unit activity from downstream SNR neurons and examined whether optogenetic stimulation of ChR2-expressing LPB_{VGLUT2} inputs is sufficient to directly excite these cells *in vivo* (Fig. 5a,b and Supplementary Fig. 2). Fifty-seven percent of the recorded SNR neurons (n = 29/53 cells) significantly increased firing with short latency (8.9 ± 0.87 ms, n = 29 cells) after light onset with no detectable changes in action potential shape (Fig. 5c–f). Further, we found that out of those SNR neurons, many were also excited by noxious stimuli (Pinch: 41.4%, n = 12/29; heat: 45.8%, n = 11/24 cells; shock: 53.3%, n = 8/15 cells; Fig. 5g,h). Interestingly, like in the LPB (Fig. 3i–p and Extended Data Fig. 3), we observed stimulus-specific responses in individual SNR neurons (Fig. 5i).

To determine brainwide axonal projections of SNR neurons targeted by LPB, we injected anterogradely-transported AAV1-Cre, which transsynaptic direction had been validated (Extended Data Fig. 7a,b), into the LPB and AAV carrying Cre-dependent eYFP into the SNR of C57BL/6 mice (n = 3 mice; Extended Data Fig. 8a). We found that LPB-targeted SNR neurons project to brain regions involved in motor control (thalamus, superior colliculus (SC), dorsal striatum and pedunculopontine nucleus (PPT)), monoaminergic centers (VTA and dorsal raphe nucleus (DR)) and descending pain modulation (periaqueductal gray (PAG)) (Extended Data Fig. 8b,c). Additionally, we observed that LPB-targeted SNR neurons send robust projections back to the LPB, innervating the LPBc (Extended Data Fig. 7c, 8b,c). The LPBc predominantly contains LPB→VTA neurons (Fig. 1e). These results are consistent with our input mapping demonstrating that LPB→VTA neurons receive substantial input from the SNR (Extended Data Fig. 2). Additional patch-clamp experiments confirmed the existence of a functional feedback loop between excitatory LPB neurons and LPB-projecting SNR neurons (Extended Data Fig. 8d–f).

We hypothesized that activation of LPB-targeted SNR neurons in response to noxious stimuli inhibits VTA DA neurons both through feedforward inhibition and by reducing excitatory drive from a separate population of LPB neurons. Further experimental data support the existence of such circuitry: first, injection of AAV1-Cre into the LPB and AAV carrying Cre-dependent synaptophysin into the SNR confirmed the presence of synaptic terminals in lateral VTA and LPBc (Fig. 6a,b). Second, patch-clamp recordings of mice injected with AAV1-Cre into the LPB and AAV carrying Cre-dependent ChR2 into the SNR revealed large light-evoked IPSCs in NAcLat-projecting DA neurons (n = 8 cells) and LPB→VTA neurons (n = 4 cells). Light-evoked IPSCs were blocked by application of a GABA-A receptor antagonist (picrotoxin, PCTX) (Fig. 6c–f). Third, optogenetic stimulation of ChR2-expressing SNR terminals produced large light-evoked IPSCs in all LPB→VTA neurons (n = 6 cells) and 20-Hz light stimulation inhibited spontaneous firing (n = 4 cells).

Light-evoked IPSCs and light-induced inhibition of firing were blocked by PCTX (Fig. 6g–i).

The divergent projections from LPB-targeted SNR neurons to VTA and LPB could originate from different SNR subpopulations or represent axon collaterals of the same neurons, but we found that LPB-projecting SNR neurons (SNR→LPB) have few if any collaterals to NAcLat-projecting DA neurons (Extended Data Fig. 9).

If LPB→VTA neurons are part of a larger brain network that involves pain-induced activation of the LPB→SNR pathway and inhibition through SNR neurons, then optogenetic activation of LPB→VTA neurons should induce a similar behavioral response as optogenetically silencing LPB→SNR neurons (Fig. 4). Because we observed fibers of passage in the VTA (Fig. 1c) that could potentially confound the interpretation of behavioral effects when activated in optogenetic terminal-stimulation experiments, we were somewhat limited in the type of optogenetic manipulations we could use. As such, we decided to employ an approach that combines rabies tracing and optogenetics to selectively activate LPB neurons that make direct monosynaptic connections onto VTA DA neurons (i.e., LPB→VTA_{DA}). We injected AAV-DIO-TVA and AAV-DIO-RG into the VTA of DAT-Cre mice, followed 3 weeks later by EnvA-RV-ChR2 or EnvA-RV-GFP and bilateral implantation of optical fibers in the LPB (Fig. 6j). Patch-clamp recordings from LPB neurons expressing ChR2 demonstrated that light stimulation induced action potentials at various frequencies, thus confirming the validity of our genetic targeting approach (Extended Data Fig. 10a–f). We then injected the mice with formalin unilaterally into the right hind paw and analyzed licking behavior while optogenetically activating LPB→VTA_{DA} neurons. We observed a reduction in pain-related licking during phase II of the formalin-test in ChR2-compared to GFP-expressing mice (Fig. 6k,l), which is consistent with the behavioral results from optogenetically silencing (Fig. 4) or ablating (Extended Data Fig. 6) LPB→SNR neurons. Moreover, optogenetic stimulation of LPB→VTA_{DA} neurons with 473 nm light did not affect general locomotor activity (Extended Data Fig. 10g–j) but induced place-preference behavior (Extended Data Fig. 10k–m).

Taken together, SNR neurons directly and indirectly target VTA DA neurons as well as other wide-ranging brain areas to serve as a critical hub for sensory, motor, and motivational control.

Role of LPB for pain-induced inhibition of DA release

To further examine the proposed circuit model *in vivo*, we combined optogenetic stimulation of SNR inputs to LPB with fiber photometry of DA terminals in NAcLat and NAc medial shell (NAcMed). We injected DAT-Cre mice with AAV-ChR2-mCherry into lateral SNR and AAV-DIO-GCaMP6m into VTA and implanted optical fibers in the NAcLat or NAcMed and above the LPB of the same animal (NAcLat: n = 6 mice, NAcMed: n = 5 mice). This enabled us to shine light over the LPB to activate SNR terminals while simultaneously recording DA terminal activity in the NAcLat or NAcMed (Fig. 7a,b and Supplementary Fig. 3a–d). We found that activation of SNR terminals in the LPB with 20 Hz stimulation significantly decreased emitted fluorescence signals in the NAcLat,

compared to fluorescence signals without optogenetic stimulation or compared to signals in the NAcMed, which were not altered in response to optogenetic stimulation (Fig. 7c–e).

Next, to test whether LPB→SNR neurons are necessary for pain-induced inhibition of DA release *in vivo*, we sought to selectively ablate LPB→SNR neurons. We bilaterally injected AAVretro-Cre into the SNR and infused AAV carrying Cre-dependent Caspase 3 unilaterally into the LPB of C57Bl/6 mice. A control virus (i.e., AAV-DIO-mCherry) was infused into the opposite LPB (n = 9 mice). In the same animals, we infused a genetically encoded DA indicator (dLight1.2)[40] bilaterally into the NAcLat and implanted optical fibers in these regions. Six weeks later, head-fixed animals were subjected to electrical shock or pinch to the animals' tail while performing fiber photometry recordings in the NAcLat (Fig. 7f and Supplementary Fig. 3e,f). In the NAcLat side that reflected infusion of the control vector into LPB, we observed an inhibition of DA release in response to shock and pinch. In the opposite NAcLat (i.e., reflecting Caspase 3 infusion into LPB), we observed a significant reduction, although not complete loss, of the shock- and pinch-induced inhibition of DA release (Fig. 7g–i).

Collectively, our results suggest a key role of LPB→SNR neurons in the pain-mediated inhibition of mesolimbic DA release; mechanistically, this process involves, at least in part, reduced excitatory drive onto VTA DA neurons.

DISCUSSION

An understanding of the neuronal basis of behavioral changes elicited by noxious stimulation requires a precise knowledge of the circuits that transmit pain-related information. Here, we describe a spino-parabrachio-mesencephalic circuit through which pain signals are transmitted from the spinal cord to VTA DA neurons (Fig. 8).

LPB links spinal cord to dopamine neurons

Our results are consistent with the growing body of evidence that neurons within the LPB relay a wide variety of noxious sensory information to forebrain structures[21,22,24–28]. Indeed, as reported previously[9,24,41], we found that a large proportion of LPB neurons are excited by nociceptive stimulation (Fig. 3). However, some LPB neurons were inhibited by noxious stimuli, and many LPB cells showed stimulus-specific responses (Extended Data Fig. 3). Given that many SNR neurons are excited in response to noxious stimuli and exert strong inhibitory influence over LPB→VTA neurons (Fig. 5 and 6), it is possible that some of the LPB neurons that are inhibited by noxious stimuli are those that project to the VTA. Furthermore, our single unit recordings of opto-tagged LPB→SNR neurons revealed a smaller proportion of cells that are inhibited by noxious stimuli (Fig. 3m–p). Likewise, cell populations throughout the ventral midbrain exhibit highly heterogeneous responses to noxious stimuli[30]. It is therefore possible that the two LPB pathways have a more complex innervation pattern with other ventral midbrain cell populations (e.g., glutamate neurons) not studied here. Nevertheless, our findings, together with other recent studies[21,24,26,28], emphasize the importance of dissecting the anatomy and functional role of different LPB subpopulations and demonstrate the utility of using a multipronged approach combining techniques to study LPB circuits on both population and single cell levels.

A previous study had proposed that pain-responsive LPB neurons may be a critical link in the transmission of pain-related information to VTA DA neurons[9], but the fact that the majority of LPB neurons are glutamatergic and are excited in response to painful stimuli, whereas most VTA DA neurons are inhibited, has posed a major challenge in our understanding of how pain-related information may reach VTA DA neurons. Our study directly addresses this issue by showing that noxious stimuli can reduce excitatory input from the LPB to VTA DA neurons. Central to this process is a circuit mechanism involving the excitation of SNR GABAergic neurons through a separate population of LPB neurons that receives direct synaptic input from the spinal cord. We argue that reduced excitatory input from the LPB to VTA DA neurons may explain at least part of the reduced activity of those neurons that has been observed in response to noxious stimuli. In addition, feedforward inhibition of VTA DA neurons via LPB-targeted SNR neurons may also contribute to the pain-induced inhibition of VTA DA neurons (Fig. 6c,d). LPB→VTA and LPB→SNR neurons might also be targeted by the vagal gut-brain axis[42,43] and therefore modulated independently of dorsal horn spinal inputs.

SNR neurons can have highly collateralized networks[34], but LPB-projecting SNR neurons have few if any collaterals to VTA DA neurons (Extended Data Fig. 9). Therefore, it is likely that separate populations of LPB-targeted SNR neurons exist which target VTA DA neurons directly via feedforward inhibition and indirectly through inhibition of LPB neurons, thereby reducing excitatory drive onto VTA DA neurons. Since genetic ablation of LPB→SNR neurons attenuates but does not completely abolish pain-induced inhibition of VTA DA neurons (Fig. 7), we cannot rule out additional inhibitory influence from other brain structures not studied here. For example, lateral habenula (LHb) neurons are excited by aversive stimuli[44] and promote indirect inhibition of VTA DA neurons via GABAergic neurons in the rostromedial tegmental nucleus (RMTg)[45,46]. On the contrary, LHb lesions do not affect transient pain-related responses in VTA DA neurons[47], but diminish inhibitory responses during the absence of an expected reward[48], suggesting that the LHb may not be the primary source that drives the pain-induced inhibition of VTA DA neurons.

Heterogeneity of dopamine neurons

The midbrain DA system is composed of anatomically and functionally heterogeneous DA subpopulations with different axonal projections[10,30,31,45]. While it has been argued that most SN DA neurons do not respond to noxious stimuli[49,50 *cf.*51], a large proportion of VTA DA neurons is inhibited by them[10–13]. However, several subpopulations of DA neurons have been discovered that show robust activation in response to aversive stimuli[10,52]. These DA neurons are clustered in the medial VTA and can be identified based on their downstream projection targets (e.g., to the ventral NAcMed[10]). They seem to represent non-canonical DA neurons that have electrophysiological and molecular properties that are largely different from classical DA neurons in the lateral VTA, which are known to be inhibited in response to aversive stimuli. Given that optogenetic stimulation of the SNR→LPB pathway reduced calcium transients in NAcLat but not in NAcMed DA terminals (Fig. 7a–e), we speculate that the spino-parabrachio-mesencephalic circuit proposed here largely participates in the pain-induced inhibitory response of lateral VTA DA neurons projecting to NAcLat. Future studies will need to further dissect this circuitry and address the critical question of how

nociceptive signals are transmitted from the spinal cord to those medial VTA DA neurons, which show excitatory responses following noxious stimuli[16].

SNR is hub for sensory, motor, and motivational control

SNR neurons show heterogeneous firing responses during motor behavior[53,54] and in response to noxious stimuli (Fig. 5), consistent with the idea that polymodal sensory and motor signals converge in the SNR[33]. Correspondingly, the SNR, which is a main output nucleus of the basal ganglia, conveys these signals to brainstem premotor networks and thalamic nuclei related to motor, premotor, prefrontal, and associative sensory cortical areas[34,54–56]. We found that both LPB→SNR and downstream SNR neurons are excited by noxious stimuli (Fig. 3 and 5). Consistent with this, we demonstrate that optogenetic silencing and genetic ablation of the LPB→SNR pathway is sufficient to attenuate pain responses in two different models of pain (Fig. 4 and Extended Data Fig. 6). While our data clearly suggest the involvement of the LPB→SNR pathway in the inhibition of DA neurons in response to pain (Fig. 7), we point out that the behavioral effects caused by optogenetic silencing or genetic ablation of the LPB→SNR pathway may also involve parallel or divergent circuits. This is rooted in the inherent nature of the SNR to serve as a critical hub for sensory-motor integration and the fact that LPB-targeted SNR neurons have widespread projections (Extended Data Fig. 8). Although the extent to which projections arise from the same or segregated SR neurons is currently unclear, it is conceivable that by inhibiting the LPB→SNR pathway we enable disinhibition of pain-related motor behavior controlled by SNR neurons projecting to superior colliculus[57]. Nevertheless, since (i) LPB-targeted SNR neurons project back to the LPB (Fig. 6a,b), (ii) SNR neurons target LPB→VTA neurons (Fig. 6e–i) and (iii) optogenetic stimulation of LPB→VTA DA neurons induces a similar behavioral response as silencing LPB→SNR neurons (Fig. 4 and 6), it is likely that the two LPB pathways described here are part of the same circuitry that transmits nociceptive signals from the periphery to VTA DA neurons.

Moreover, if we take into account the fact that a large proportion of VTA DA neurons play a critical role in reward-dependent behavior and learning, and that inhibition of VTA DA neurons contributes to negative reward prediction error and promotes behaviors associated with aversion[2,3,12], it is likely that the spino-parabrachio-mesencephalic circuit defined here contributes to the aversive motivational qualities of pain and to the negative reinforcement associated with pain relief. Possible parallel circuits pertinent to the aversive aspects of pain may involve the anterior cingulate cortex[37], nociceptive ensembles in the basolateral amygdala[58] and central nucleus of the amygdala, and the latter also receives prominent input from the LPB[27], although from an anatomically distinct cell population (Fig. 1d–f).

Spino-parabrachio-mesencephalic circuit in chronic pain

The spino-parabrachio-mesencephalic circuit proposed here may also be involved in the pathophysiology of chronic pain, given that optogenetic inhibition of the LPB→SNR pathway reduces pain responses in an animal model of neuropathic pain (Fig. 4). Consistent with this are multiple lines of evidence showing that chronic pain involves hypodopaminergic conditions[5,15,59,60], which may decrease reward responsivity and contribute to several of the comorbid symptoms of chronic pain patients such as reduced

motivation and depression[18,19]. While future studies will be needed to provide a more detailed understanding of how synaptic plasticity and other circuit adaptations at distinct nodes of the spino-parabrachio-mesencephalic circuit contribute to the transition from acute to chronic pain, our results advance the current understanding of how noxious stimuli affect learning and motivation through actions on mesolimbic DA neurons and provide precise anatomical and functional information that are important for the discovery and development of new pain therapies.

METHODS

Subjects

The following mouse lines (25–30 g, 8–12 weeks old, male) were used for the experiments: C57BL/6J mice (Jackson Laboratory), DAT-IRES-Cre (Jackson Laboratory, stock number: 006660, strain code: *B6.SJL-Slc6a3*$^{tm1.1(cre)Bkmn}$*/J*), VGLUT2-IRES-Cre (Jackson Laboratory, stock number: 016963, strain code: *Slc17a6*$^{tm2(cre)Lowl}$*/J*), GAD2-IRES-Cre (Jackson Laboratory, stock number: 010802, strain code: *Gad2*$^{tm2(cre)Zjh}$*/J*), VGAT-IRES-Cre (Jackson Laboratory, stock number:028862, strain code: *B6J.129S6(FVB)-Slc32a1*$^{tm2(cre)Lowl}$*/MwarJ*), Ai14 Cre reporter mice (Jackson Laboratory, stock number: 007908, strain code: *B6;129S6 Gt(ROSA)26Sor*$^{tm14(CAG-tdTomato)Hze}$*/J*). GAD2-Cre-tdTomato: Ai14 Cre reporter mice were crossed to GAD2-IRES-Cre mice. For *ex vivo* patch-clamp recordings shown in Figure 1g–m and Figure 2a–d male and female mice were used, but no significant differences were observed between male and female mice. Mice were maintained on a 12:12 light cycle (lights on at 07:00) with water and food *ad libitum* and room temperature of 22–25°C and 55% humidity. All procedures complied with the animal care standards set forth by the National Institutes of Health and were approved by University of California Berkeley's Administrative Panel on Laboratory Animal Care.

Stereotaxic Surgeries

All stereotaxic surgeries were performed under general ketamine–dexmedetomidine anesthesia using a stereotaxic instrument (Kopf Instruments, Model 1900).

Fluorescent retrobead- or fluorogold retrograde tracing—Mice were injected unilaterally with red fluorescent retrobeads (100 nl; LumaFluor Inc.) into the nucleus accumbens (NAc) lateral shell (NAcLat, bregma: 0.98 mm, lateral: 2.00 mm, ventral: −4.50 mm), ventral tegmental area (VTA, bregma: −3.40 mm, lateral: 0.40 mm, ventral: −4.50 mm) or LPB (bregma: −5.20 mm, lateral: 1.25 mm, ventral: −3.60 mm). Fluorogold (FG, 50 nl, diluted with saline, 4%; Santa Cruz Biotech.) was injected into substantia nigra pars reticulata (SNR, bregma: −3.40 mm, lateral: 1.50 mm, ventral: −4.90 mm) or lateral parabrachial nucleus (LPB; 50 nl; bregma: −5.20 mm, lateral: 1.25 mm, ventral: −3.60 mm).

Viral vectors—The AAVs (adeno associated viruses) used in this study were from the Deisseroth laboratory (AAV5-EF1a-DIO-eNpHR3.0-eYFP; pAAV5-CAG-hChR2(H134R)-mCherry.WPRE.SV40; AAV5-EF1α–DIO-hChR2(H134R)-eYFP; AAV5-EF1α-DIO-eYFP; AAV5-EF1α-DIO-mCherry; AAV5-CaMKII-ChR2-eYFP; AAVDJ- EF1α-DIO-GcAMP6m; AAV5-hSyn-hChR2(H134R)-eYFP; ~10^{12} infectious units per ml, prepared by the

University of North Carolina Vector Core, Addgene or the Stanford Gene Vector and Virus Core) or from the Uchida laboratory (Harvard University; AAV5-flex-RG; AAV5-flex-TVA-mCherry; ~10^{12} infectious units per ml, prepared by the University of North Carolina Vector Core Facility). AAV5-Caspase 3 (CASP) was from Shah & Wells laboratory (Stanford &UCSF; pAAV-flex-taCasp3-TEVp; ~10^{12} infectious units per ml, prepared by the Addgene). pAAV-hSyn-dLight1.2 (AAV5) was from Tian lab (UC Davis, ~10^{12} infectious units per ml, prepared by Addgene). AAVretro and rabies virus were from Douglas Kim & GENIE Project (Janelia Research Campus; AAVretro-hSyn-jGCaMP7f-WPRE, pENN.AAV.hSyn.Cre.WPRE.hGH (AAV retrograde) and pAAV.CMV.HI.eGFP-Cre.WPRE.SV40; ~10^{12} infectious units per ml, prepared by Addgene) and from Callaway laboratory (Salk Institute; RV-EnvA-ΔG-ChR2-mCherry (RV-ChR2); ~10^{8} infectious units per ml or RV-EnvA-ΔG-GFP (RV-GFP); ~10^{7} infectious units per ml, respectively, prepared by the Gene Transfer, Targeting and Therapeutics core of Salk Institute). pENN.AAV.hSyn.Cre.WPRE.hGH (AAV1-Cre anterograde) was from James M. Wilson laboratory (University of Pennsylvania; ~10^{13} infectious units per ml, prepared by Addgene); Canine adenovirus type 2 (CAV2-Cre) was from Plateforme de Vectorologie de Montpellier. RG-EIAV-Cre was prepared by the Lim laboratory (UC San Diego). AAV8.2-hEF1α-DIO-synaptophysin-mCherry was prepared by MIT Vector Core (~10^{13} infectious units per ml).

Viral injections—200–500 nl of AAV was injected into LPB (200 nl; bregma:−5.20 mm, lateral: 1.25 mm, ventral: −3.60 mm), SNR (400 nl; bregma: −3.40 mm, lateral: 1.50 mm, ventral: −4.90 mm), VTA (500 nl; bregma: −3.40 mm, lateral: 0.40 mm, ventral: −4.50 mm), dorsal horn (400 nl, L4–5) or NAcLat (300 nl, bregma: 0.98 mm, lateral: +/−2.00 mm, ventral: −4.20 mm) using a syringe pump (Harvard Apparatus) at 150 nl/min. For CAV2-Cre tracing in Ai14 mice (Fig. 1d–f, 2a–d and Extended Data Fig. 7a), 200–300 nl of CAV2-Cre, (diluted with PBS, 3:1), was injected into VTA (300 nl; bregma: −3.40 mm, lateral: 0.40 mm, ventral: −4.50 mm) or SNR (300 nl; bregma: −3.40 mm, lateral: 1.50 mm, ventral: −4.90 mm), or central nucleus of the amygdala (CeA) (300 nl; bregma: −1.40 mm, lateral: 2.80 mm, ventral: −4.75 mm) or LPB (200 nl; bregma: −5.20 mm, lateral: 1.25 mm, ventral: −3.60 mm). For genetic ablation, 400 nl RG-EIAV-Cre (Extended Data Fig. 6) or 300 nl AAVretro-Cre (Fig. 7f–i) was injected into SNR (bregma: −3.40 mm, lateral: +/−1.50 mm, ventral: −4.90 mm; bilateral: Fig. 7f–i; unilateral: Extended Data Fig. 6) and pAAV-flex-taCasp3-TEVp (300 nl; mixed with control virus (i.e., AAV-DIO-mCherry or AAV-DIO-eYFP), 1:1) was injected into LPB (bregma: −5.20 mm, lateral: 1.25 mm, ventral: −3.60 mm) of same animal.

Experiments were performed 4–8 weeks (for AAVs), 10–13 days (RV-ChR2), 3 weeks (for CAV2-Cre and AAV1-Cre) or 2–7 days (for retrograde tracers) after stereotactic injection. Injection sites and optical fiber placements were confirmed in all animals by preparing coronal sections (50–100 μm) of injection- and implantation sites. We routinely carried out complete serial reconstruction of the injection sites and optical fiber placements. Although optical fiber placements varied slightly from mouse to mouse, behavioral data from all mice were included in the study.

In vivo optogenetic experiments—AAV5-ChR2-injected mice received unilateral implantation of a chronically-implanted optical fiber (200 μm, NA = 0.37; Newdoon Inc.) dorsal to the LPB (bregma: −5.2 mm, lateral: 1.25 mm, ventral: −3.20 mm) or SNR (bregma: −3.40 mm, lateral: 1.50 mm, ventral: −4.50 mm); RV-ChR2 and NpHR-injected mice received bilateral implantations of optical fibers dorsal to the LPB (bregma: −5.2 mm, lateral: ±1.25 mm, ventral: −3.20 mm) or SNR (bregma: −3.40 mm, lateral: ±1.50 mm, ventral: −4.50 mm), respectively.

In vivo fiber photometry experiments—Mice received unilateral or bilateral implantation of a chronically-implanted optical fiber (400 μm, NA = 0.48; Newdoon Inc.) in the LPB (bregma: −5.20 mm, lateral: 1.25 mm, ventral: −3.40 mm), nucleus accumbens (NAc) ventromedial shell (NAcMed, bregma: 1.50 mm, lateral: +/−0.90 mm, ventral: −4.80 mm) or NAc lateral shell (NAcLat, 0.98 mm, lateral: +/−2.00 mm, ventral: −4.20 mm).

Electrophysiology

Ex vivo electrophysiology—Mice were deeply anaesthetized with pentobarbital (200 mg/kg intraperitoneal; Vortech). Coronal slices of the VTA and SNR or LPB (200 μm) were prepared after intracardial perfusion with ice-cold artificial cerebrospinal fluid (ACSF) containing (in mM) 50 sucrose, 125 NaCl, 25 $NaHCO_3$, 2.5 KCl, 1.25 NaH_2PO_4, 0.1 $CaCl_2$, 4.9 $MgCl_2$, and 2.5 glucose (oxygenated with 95% O_2/5% CO_2). After 90 min of recovery, slices were transferred to a recording chamber and perfused continuously at 2–4 mL/min with oxygenated ACSF (bath solution) containing (in mM) 125 NaCl, 25 $NaHCO_3$, 2.5 KCl, 1.25 NaH_2PO_4, 11 glucose, 1.3 $MgCl_2$ and 2.5 $CaCl_2$. Cells were visualized with a 40x water-immersion objective on an upright fluorescent microscope (BX51WI; Olympus) equipped with infrared-differential interference contrast video microscopy and epifluorescence (Olympus). Patch pipettes (3.8–4.4 MΩ) were pulled from borosilicate glass (G150TF-4; Warner Instruments).

For recordings of light-evoked inhibitory postsynaptic currents (IPSCs), patch pipettes were filled with internal solution containing (in mM) 130 CsCl, 1 EGTA, 10 HEPES, 2 MgATP, 0.2 NaGTP, 0.1% neurobiotin pH 7.35 (270–285 mOsm). 20 μM CNQX (6-cyano-7-nitroquinoxaline-2,3-dione, Bio-tech) and 50 μM D-AP5 (Tocris) was added to the bath solution to block AMPA and NMDA receptors, respectively. The voltage-gated sodium channel antagonist tetrodotoxin (TTX, 1 μM, Hello Bio) and the potassium channel antagonist 4-aminopyridine (4-AP, 1 mM, Sigma) were also added to the bath solution to isolate monosynaptic inputs. For recordings of light-evoked excitatory postsynaptic currents (EPSCs), the internal solution contained (in mM) 117 CsCH3SO3, 20 HEPES, 0.4 EGTA, 2.8 NaCl, 5 TEA, 4 MgATP, 0.3 NaGTP, 5 QX314, 0.1 Spermine, pH 7.35 (270–285 mOsm). 100 μM picrotoxin (PCTX, Sigma) was added to the bath solution to block inhibitory currents mediated by GABAA receptors as well as TTX (1 μM) and 4-AP (1 mM). Miniature excitatory postsynaptic currents (mEPSCs) were recorded in the presence of 1 μM TTX and 100 μM PCTX and miniature inhibitory postsynaptic currents (mIPSC) were recorded in the presence of 1 μM TTX, 20 μM CNQX and 50 μM D-AP5; cells were recorded for 5 min. For recordings of spontaneous firing, the internal solution contained (in mM) 135 K-gluconate, 5 KCl, 10 HEPES, 0.1 EGTA, 2 $MgCl_2$, 2 MgATP, 0.2 NaGTP, and

0.1% neurobiotin, pH 7.35 (290–300 mOsm). Cells were held in current clamp mode and no current injections were made. Spontaneous firing was recorded for at least 3 s before and 5 s after light stimulation (5 to 40 Hz (Extended Data Fig. 10d), 10 Hz (Fig. 1l,m) or 20 Hz (Fig. 6i), 5 ms light pulses, 5 mW/mm^2) and averaged over 10 sweeps. For pharmacological experiments, baseline responses were recorded for at least 3–5 min and then 20 μM CNQX, 50 μM D-AP5 or 100 μM PCTX was added to the bath solution for 5–10 min. Electrophysiological recordings were performed at 32°C using a MultiClamp700B amplifier and acquired using a Digidata 1440A digitizer, sampled at 10 kHz, and filtered at 2 kHz. ChR2 was stimulated by flashing 473 nm light through the light path of the microscope using an ultrahigh-powered light-emitting diode (LED) powered by an LED driver (Prizmatix) under computer control. The light intensity of the LED was not changed during the experiments and the whole slice was illuminated (5 mW/mm^2). Light-evoked EPSCs or IPSCs were obtained every 10 s with one pulse of 473 nm light (5 ms) with neurons voltage clamped at −70 mV. Series resistance (15–25 MΩ) and input resistance were monitored online. Data were analyzed offline using Clampfit 10.6 (Molecular Devices) or IgorPro 5.0.4.8 (Wavemetrics). Light-evoked EPSC or IPSC amplitudes were calculated by averaging responses from 10 sweeps and then measuring the peak amplitude in a 50 ms window after the light pulse. For detecting mEPSC or mIPSC events, Clampfit 10.6 (Axon Instruments, Inc.) was used.

Retrobead-labeled NAcLat-projecting DA or GAD2-tdTomato-positive neurons were recorded in both the caudal and rostral VTA. The caudal VTA contained at least some parts of the rostromedial tegmental nucleus (RMTg). The boundary between the VTA and RMTg is difficult to determine, particularly in the caudal VTA, which makes it difficult to determine with certainty whether some of the recorded GAD2-tdTomato-positive neurons are in the VTA or RMTg. Thus, when referred to in the text, the VTA includes the RMTg[61].

To determine the locations and neurochemical identity, cells were filled with neurobiotin (NB, Vector) during patch-clamp recordings, then fixed in 4% paraformaldehyde (PFA) and 24 hours later immunostained for tyrosine hydroxylase (TH). All recorded retrobead-labeled NAcLat-projecting neurons were TH-immunpositive (Extended Data Fig. 1t), all SNR neurons were TH-immunonegative (Extended Data Fig. 1u) and all GAD2-tdtomato-positive neurons were TH-immunonegative (Extended Data Fig. 1v). For recordings in the LPB, cells were filled with NB to determine the precise anatomical location of the recorded cells, but no TH-immunostaining was performed (Fig. 6g).

Because most LPB neurons are excitatory, there is a possibility of recurrent excitation during *in vivo* opto-tagging[62]. Hence, patch-clamp recordings were performed to analyze light response latency threshold distributions. ChR2-expressing (i.e., ChR2-positive) and non-ChR2-expressing (ChR2-negative) LPB neurons were recorded and post hoc neurobiotin histochemistry of the recorded neurons was performed. ChR2-expresssing LPB neurons showed a constant inward current response to 1-sec constant blue laser light in the voltage-clamp configuration (n = 23 cells). Conversely, non-ChR2-expressing LPB cells did not respond to light stimulation (n = 10 cells). n = 4 LPB cells did not express ChR2, but still responded to light stimulation. However, these cells had mean light response latencies

of 16.9 ms (range: 13.1–22.3 ms), which was longer than light responsive, ChR2-positive neurons (mean: 6.4 ms; range: 1.5–11.7 ms) (Supplementary Fig. 1c–g).

In vivo electrophysiology—Animals were implanted with a custom-built optrode above the LPB (bregma: −5.2 mm, lateral: 1.25 mm, ventral: −3.0 mm) or SNR (bregma: −3.4 mm, lateral: 1.5 mm, ventral: −4.5 mm), which consisted of eight tetrodes (12 μm polyimide-coated NiCr wire protected by silica tubing) glued to a 200 μm optical fiber using epoxy. The tetrodes protruded from the tip of the optical fiber by ~0.5 mm. Wire tips were cut flat and gold plated to reduce impedance to ~200 kΩ at 1 kHz. A small screw fixed to the skull served as a ground electrode. Data collection began one week after the optrode implantation. Neural signals were recorded using a Digital Lynx 4SX system with HS-18-MM headstage pre-amplifier (Neuralynx). Recorded signals were filtered between 0.6 and 6 kHz and sampled at 32 kHz. Spikes were sorted offline using SpikeSort3D 2.5.4 (Neuralynx) software. At the end of each recording session, the optrode was moved ventrally for ~40 μm. The final recording location was verified using histology after the electrolytic lesions (12 μA, 30 s).

ChR2-tagged neurons were identified by delivering 473 nm (0.8 mW/mm^2, 5 ms pulses) light at 1 Hz frequency for 2–3 min. A 2 ms bin with the highest number of spikes in the interval [0, +100 ms] around the laser pulse was identified. To test if the identified strongest response to light was higher than chance, we shuffled all the spike times in the same [0, +100 ms] interval 10,000 times and counted the highest number of spikes in a 2 ms bin for each iteration. If the number of spikes in the 2 ms bin from the real data exceeded the 99.9th percentile value of the distribution of number of spikes in the most active 2 ms bin for the shuffled data, we classified the cell as light responsive. Response latency was defined as the average response time in the most active 2 ms bin (Fig. 3k; adapted from ref.[63]).

For noxious stimulation (Fig. 3m–p, 5g–i and Extended Data Fig. 3): Tail pinch: Mice received 10–15 tail pinches using forceps (3–4 cm from tip of the tail, 5 s duration, 30–60 s intervals between pinches). Heat: The tip of the tail was placed in a temperature-controlled water bath (50°C, 10 s duration, 60 s intervals, 7–10 trials). Electrical shock: Electrode gel (Spectra 360, Parker Laboratories) was placed on the tail and mice received 15–20 0.5 mA tail shocks (manual generator, 0.5 mA each, 200 ms duration, 30 s intervals) or 36 0.5 mA tail shocks (automatic generator, 0.5 mA each, 50 ms duration, 5 s intervals). The experimental time stamps were acquired using a manual TTL pulse generator or a Master-8 pulse stimulator (A.M.P.I). To determine whether noxious stimuli altered neural activity patterns (i.e., excitation, inhibition, no response), 2 sec baseline mean firing rate before the noxious stimulus were compared to the mean firing rate during the noxious stimuli using paired t-tests ($p < 0.05$: excited or inhibited, $p > 0.05$: non-responder). For electrical shock, a post-interval epoch of 500 ms was analyzed to avoid potential interference with the electrical stimulus.

Fiber photometry

Calcium transients were measured using a custom-built fiber photometry rig as described previously[10,64]. Briefly, fluorescence signals were obtained by stimulating cells expressing

GCaMP6m or dLight1.2 with a 470 nm LED (20 μW at fiber tip), while calcium-independent signals were obtained by stimulating these cells with a 405 nm LED (20 μW at fiber tip). 470 nm and 405 nm LED light was alternated at 20 Hz and light emission was recorded using a sCMOS Camera (Photometrics Prime), which acquired video frames containing the fiber bundle (2 fibers, 1 m in length, NA = 0.48, 400 μm core, Doric Lenses) at the same frequency. Video frames were analyzed online and fluorescent signals were acquired using custom acquisition code written in Matlab (R2019b) [10]. All fiber photometry experiments were performed in head-fixed mice.

For fiber photometry recordings in Fig. 3a–h: Tail shock: Electrode gel (Spectra 360, Parker Laboratories) was placed on the tail and mice received eight 0.5 mA tail shocks (0.5 mA each, 2 s duration, 30 s intervals between shocks). Tail shock timestamps were acquired using TTL pulses generated by a Master-8 pulse stimulator (A.M.P.I.). Tail pinch and tail brush: Mice received eight tail pinches or brushes (3–4 cm from tip of the tail) using forceps or brush, respectively (1 s duration, 30–60 s intervals between pinches). Hot water test: The tip of the tail was placed in a temperature-controlled water bath ranging from 40°C to 55°C (20 s duration, 120 s intervals between each temperature level). Tail pinch, tail brush and thermal stimuli were applied manually, and experimental timestamps were acquired using a manual TTL pulse generator, which were then synchronized to calcium recordings at the designated time during the recording. Calcium signals were normalized (Z-score) and peri-event plots for tail shock, pinch and brush were generated. AUC for the hot water test was defined as the integral between 0 and 20 s.

For fiber photometry recordings in Fig. 7a–e: To prevent overlap between ChR2 and GCaMP signals, we used ChR2 that was fused to mCherry and light at very low intensities: GCaMP excitation was performed using LED light intensities at 20 μW in NAcMed or NAcLat and < 3 mW for ChR2 excitation in LPB. In 100 s intervals, mice received laser light stimulation for 5 s at 20 Hz (5 ms pulse-width) in LPB while we recorded calcium fluorescence signals from DA terminals in NAcMed or NAcLat. 20–24 trials were averaged per animal. The AUC interval was defined as the entire laser stimulation period (0–5 s).

For fiber photometry recordings in Fig. 7f–i: For noxious stimulation 0.5 mA electrical shocks (2 s duration) or tail pinches (5 s duration) were delivered to animals' tails (15–20 trials).

Behavioral Assays

Open field test—It was conducted to measure the effect of optogenetic stimulation on general locomotor activity[31]. Mice with fiberoptic implants were connected to a fiberoptic cable and placed in an open field box (50 × 50 × 50 cm)[45]. The cable was connected to either a 473 nm or a 589 nm DPSS laser (Laserglow) through a rotary adaptor, and laser output was controlled using a Master-8 pulse stimulator (A.M.P.I.). The movement of the animals was recorded and analyzed by using video tracking software (Biobserve 3.0.1.442). A 9-min session was divided into three epochs (each 3 min): 3 min light off; 3 min light on (10 or 20 Hz of 473 nm light (5 ms pulses) for ChR2-expressing mice or continuous 589 nm light for NpHR-expressing mice); 3 min light off. The inner zone of the open field box was defined as the 23 × 23 cm central square area. Mice typically spend very little time in the

inner zone; however, in mice that display a robust anxiolytic phenotype, this time would be increased[65]. Laser power output was 0.8–1.5 mW/mm^2 (ChR2) or 3–5 mW/mm^2 (NpHR). For the genetic ablation experiment (Extended Data Fig. 6c), mice were placed in the box for 10 min and the total distance traveled was analyzed.

Real-time (RT) place preference test—Mice with fiberoptic implants were connected to a fiberoptic cable and placed in a custom-made chamber with three compartments[45]. The cable was connected to a 473 nm DPSS laser diode (Laserglow) through a rotary adaptor and laser output was controlled using a Master-8 pulse stimulator (A.M.P.I.). Power output for the cable was tested using a digital power meter (Thorlabs) and was checked before and after each experimental animal; output during light stimulation was estimated to be 0.8–1.5 mW/mm^2. One randomly assigned side of the chamber was assigned as the initial stimulation side (Phase 1), and after 10 min the stimulation side was switched to the previously non-stimulated side of the chamber (Phase 2). At the start of each session, the mouse was placed in the neutral (middle) compartment, and every time the mouse crossed to the stimulation side, 20 Hz (5 ms pulses) laser stimulation was delivered until the mouse crossed back into the neutral, non-stimulation side. There was no interruption between Phase 1 and Phase 2. The movement of the mice was recorded via video tracking software (Biobserve 3.0.1.442) and the time spent in each area (stimulated, non-stimulated, and neutral) was calculated.

Conditioned place preference (CPP)—The CPP test consisted of 5 sessions over 5 days and was performed in the same chamber as described above for RT place preference[45]. On day 1, individual mice were placed in the neutral (middle) compartment and allowed to freely explore the entire apparatus for 20 min (pre-test). On days 2–4, mice were confined to one of the side chambers (conditioned compartment) for 30 min during optical stimulation with 589 nm light (continuous light, 5 mW/mm^2). During days 2–4, mice were also placed in the opposite side chamber (unconditioned compartment) for 30 min, but without any light stimulation. Both the order the animals were placed in the conditioned versus unconditioned compartment and the side (context) were counterbalanced across animals. On day 5, like day 1, mice were placed in the middle compartment and allowed to explore the entire apparatus for 20 min (post-test). Video tracking software (Biobserve v3.0.1.442) recorded all animal movements and time spent in each compartment during the pre- and post-tests. To calculate preference or aversion, the time animals spent in the conditioned compartment during the pre-test was subtracted from the time they spent in the same compartment during the post-test.

Sciatic Nerve Legation (SNL) model—Mice were deeply anaesthetized with isoflurane and placed on a thermoregulated heating pad at 37°C. All surgical instruments were sterilized before surgery. The surgical area from slightly below the knee to hip was shaved and sterilized with antiseptic solution. An incision was made in the thigh parallel and the sciatic nerve was exposed and separated from the surrounding connective tissue by curved blunt-tipped forceps and micro-scissors under the microscope (Olympus), and approximately one-third to one-half the diameter of the sciatic nerve was tightly ligated with 6–0 silk ligature (AD surgical). For sham controls, the sciatic nerve was exposed

on the opposite side, but no ligation was performed. The incisions were closed with a tissue adhesive (Vetbond; 3M) and 1–4 absorbable sutures (AD Surgical). The nerve and surrounding wound were kept moist with saline throughout the surgery.

Formalin test—Formalin is a noxious chemical that induces inflammatory pain[66]. Formalin solution was prepared from commercially available stock formalin (contains 37% formaldehyde, Sigma) by further diluting it with isotonic saline to reach 1% concentration. 50 μl of 1% formalin was injected subcutaneously into the plantar surface of the hindpaw (unilateral: Fig. 4a–d, 6j–l and Extended Data Fig. 4; bilateral: Extended Data Fig. 6) were performed. Formalin was injected as quickly as possible using a 30-gauge needle (EXEL). Mice displayed spontaneous pain behavior, characterized by increased paw flinching, licking, and keeping the paw elevated as originally described by refs.[66,67]. For c-Fos experiments (Extended Data Fig. 4), control mice received a 50 μl saline injection subcutaneously into the plantar surface of the hind-paw. Mice were then placed into a transparent plastic box (W × L × H: 20 × 20 × 50 cm) and the animals' behavior was recorded on video. Behavioral scoring began 1 min after injections and continued for 40 min. A trained rater scored pain-related behavior by recording the number and duration of paw licks occurring during 1 min periods from 1 to 40 min after formalin injection. Phase I was defined as the time between 0–5 min and Phase II was defined as the time between 5–40 min. Phase I is typically considered the result of chemical activation of nociceptors, while Phase II reflects the inflammatory reaction and central processing[68]. For optogenetic silencing, continuous 589 nm light (5 mW/mm^2) was used (Fig. 4a–d). For optogenetic stimulation, 1.5 mW/mm^2 473 nm light (20 Hz, 5ms) was used (Fig. 6j–l). The rater was blind to NpHR- or ChR2- versus eYFP- or GFP-expressing mice.

Von Frey test—It was used to determine the mechanical sensory threshold[69]. 50% paw withdrawal threshold (PWT) in response to Von Frey stimuli was measured by using the Up-Down method[70,71]. Mice were placed in a transparent plastic box (W × L × H, 20 × 20 × 50 cm) with a metal grid (1.0 × 1.0 cm) floor to habituate for 20 min. A series of eight Von Frey filaments (4.74 (6.0 g), 4.56 (4.0 g), 4.31 (2.0 g), 4.08 (1.0 g), 3.84 (0.6 g), 3.61 (0.4 g), 3.22 (0.16 g), 2.83 (0.07 g; Stoelting)), which increased in force with approximately equal logarithmic value (δ; 0.27), were gently applied perpendicularly to the plantar surface of each hind paw until the filament bent (for ≤ 2 s). A positive response included brisk paw withdrawal, flinching, licking, or shaking. Testing began with the filament 4.08 (1.0 g) and when a positive response occurred to a stimulus, the next smaller Von Frey filament was applied. When a negative response occurred, the next higher filament was applied. To calculate the optimal threshold using this method requires six responses closest to the 50% threshold. Although all responses were noted, counting of the critical six data points did not begin until the response threshold was first crossed, at which time the two responses straddling the threshold were retrospectively designated as the first two responses of the series of six responses. Four additional responses to the continued presentation of stimuli that were varied sequentially up or down, based on the animals' response, constituted the remainder of the series. The pattern of positive and negative responses was converted to 50% threshold according to the formula: $50\%\ \text{threshold}\ (g) = \left(10^{[X_f + K\delta]}\right)/10000$, in which X_f represented the value of the final Von Frey filament used and K was correction factor

for the pattern of positive/negative responses. The experimenter was blind to NpHR versus eYFP mice and SNL versus sham mice.

Hot plate test—It was used to measure thermal nociception[69]. Mice were placed on a hot plate analgesia meter (Harvard Apparatus), which has a thick aluminum plate (10 mm) providing a high temperature stability and even surface distribution. The latency to a nociceptive heat response at 50°C (± 0.1°C) was recorded, defined as the time elapsed until the subject licks or flicks its hind paw (Fig. 4j). For quantification of c-Fos expression, mice were exposed to two different temperature conditions (37° and 55°C; Extended Data Fig. 4). The experimenter was blind to NpHR- versus eYFP-expressing mice and mice exposed to different temperature conditions.

Licking behavior—Mice with fiberoptic implants were connected to a laser, placed in an operant conditioning chamber with a drinking spout (24 cm W × 20 cm D × 18 cm H, Med Associates) and habituated for 1 hour. Animals could consume 1% (wt/vol) sucrose solution during this time. On the following day, mice were water deprived and reintroduced to the chamber for 30 min. Mice could again consume 1% (wt/vol) sucrose solution but received optical stimulation with 589 nm light (continuous light, 5 mW/mm^2) during the 30 min experimental phase. The drinking spout was connected to a lickometer, which recorded the number and duration of licks (NpHR: n = 8 mice, eYFP: n = 6 mice).

Two photon fluorescence micro-optical section tomography (2p-fMOST) imaging

For fMOST imaging, VGLUT2-Cre mice (n = 5 mice) were injected unilaterally with 100 nl AAV5-EF1α-DIO-eYFP into the LPB (bregma: −5.2 mm, lateral: 1.25 mm, ventral: −3.6 mm); 5 weeks later, mice were perfused with PBS followed by 4% PFA and brains were dissected and post-fixed in 4% PFA for 24 hours at 4°C. After fixation, the brains were rinsed overnight at 4 °C in 0.01 M PBS and subsequently dehydrated in a graded ethanol series (50, 70 and 95%, 1 hour at each concentration) at 4°C. After dehydration, the brains were immersed in a graded glycol methacrylate (GMA) series (Ted Pella Inc.), including 0.2% Sudan black B (SBB, 70% (2 hours), and 85% (2 hours), and 100% (overnight) at 4° C). Subsequently, the samples were impregnated in a prepolymerization GMA solution for 3 days at 4°C and embedded in a vacuum oven at 48°C for 24 hours. The embedded brains were imaged under an fMOST microscope at a voxel resolution of 0.3 × 0.3 × 1 μm^3 in Britton Chance Center for Biomedical Photonics at HUST University. The mosaics of each coronal section were stitched to obtain an entire section based on accurate spatial orientation and neighboring overlap. Equalizing the brightness of the different coronal sections was performed for axial illumination correction by quantifying the average grayscale values of the images. Image preprocessing was implemented in C++ (v17) and optimized in parallel using the Intel MPI Library (v3.2.2.006, Intel)[72].

Mapping of monosynaptic inputs using rabies virus

Rabies virus tracing[73] was used to map monosynaptic inputs to LPB subpopulations (Extended Data Fig. 2). VGLUT2-Cre mice were injected with 150 nl AAV-FLEX-TVA (a cellular receptor for subgroup A avian leukosis viruses) and 150 nl AAV-FLEX-RG (rabies virus glycoprotein) into the LPB. 4 weeks later, 300 nl RV-EnvA-ΔG-GFP (glycoprotein

deficient, GFP-expressing rabies virus with the envelope protein from avian ASLV type A) was injected into the VTA or SNR. 7 days after injection, mice were perfused with 4% PFA in PBS. Brains were stored in 10% sucrose in PBS at 4°C overnight and then processed for analysis. For input mapping, 100 μm sections of the whole brain were prepared and imaged using an Axio Imager 2 microscope (Zeiss). GFP-expressing input cells to LPB→VTA or LPB→SNR neurons were counted manually. Animals were randomized and investigators were blinded to group allocation (i.e., projection target).

For analyzing collateralization of LPB-projecting SNR neurons (Extended Data Fig. 9), DAT-Cre mice were injected with 150 nl AAV-FLEX-TVA and 150 nl AAV-FLEX-RG into VTA. 4 weeks later, 300 nl RV-EnvA-ΔG-GFP was injected into the NAcLat and 50 nl Fluorogold (4%) to LPB; 7 days after injection, mice were perfused and 100 μm brain sections were collected. SNR-containing brain sections were imaged using an Axio Image 2 microscope (Zeiss).

Immunohistochemistry

Immunofluorescence and confocal microscopy were performed as described previously[45,74] and in Supplementary Methods.

Statistics

Student's t tests (paired and unpaired) and one- or two-way RM ANOVA tests were used to determine statistical differences for anatomical, behavioral, and electrophysiological data using GraphPad Prism 8.4.3 (Graphpad Software). Tukey's post hoc test or Holm-Sidak's post hoc analysis was applied when ANOVA showed a significant main effect. Details of the statistical analysis are summarized in Supplementary Table 1. ∗ $p < 0.05$, ∗∗ $p < 0.01$, ∗∗∗ $p < 0.001$. All data are presented as means ± SEM. No statistical method was used to predetermine sample size but our sample sizes are similar to those reported in previous publications[10,31]. No data were excluded from the analyses and experimental and control animals were randomized throughout the study. Investigators were blind to allocation of groups and outcome assessment for experiments in Fig. 4, 6j–l, 7f–i and Extended Data Fig. 2, 4, 5c–h, 6, 10g–m. All other experiments were not blind because the experimental conditions were obvious to the researchers and the analysis were performed objectively and not subjective to human bias or analyses were automated. All experiments were independently replicated in at least 2 cohorts of animals (n number of each experimental group is reported in Supplementary Table 1). Image analyses of Extended Data Fig. 1p–s, 7a–c were replicated in 2 animals, all of others imaging experiments were replicated in at least 3 animals.

Data availability

The datasets generated during and/or analyzed during the current study are available from the corresponding author on reasonable request.

Code availability

All custom code used for analysis in this manuscript is available on request.

Extended Data

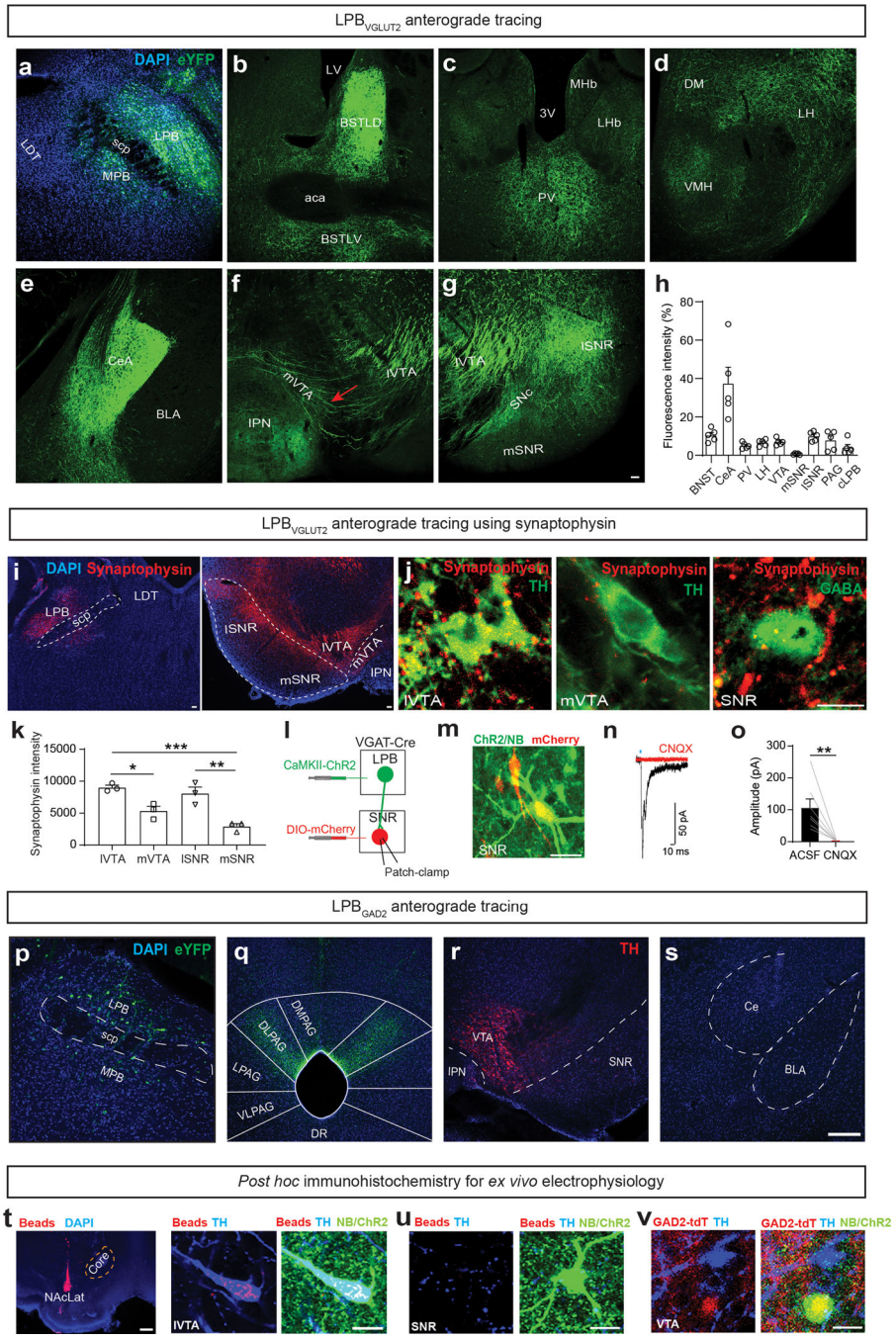

Extended Data Fig. 1. Neuroanatomical characterization of LPB→SNR and LPB→VTA neurons.

(a) eYFP-expressing LPB$_{VGLUT2}$ neurons. **(b-g)** LPB$_{VGLUT2}$ terminals expressing eYFP in different brain regions. Bregma: 0.14 mm (b), −1.22 mm (c), −1.46 mm (d), −1.46 mm (e), 3.40 mm (f), −3.40 mm (g). Note fibers of passage in VTA (red arrow) (scale bar 50 μm). **(h)** Mean eYFP fluorescence intensity in different brain areas (n = 5 mice; Data represent mean ± SEM). **(i)** Synaptophysin-mCherry expression in LPB (left) and

ventral midbrain (right) from VGLUT2-Cre mice (scale bars 50 μm). **(j)** High resolution images of synaptophysin-expressing LPB_{VGLUT2} terminals close to lateral VTA (lVTA) TH-immunopositive and SNR GABA-immunopositive neurons (scale bar 20 μm). **(k)** Mean synaptophysin intensity (quantified as number of particles in a defined region) for different ventral midbrain subregions (n = 3 mice). **(l)** Experimental design. **(m)** Sample of a recorded and neurobiotin (NB)-filled, mCherry-positive SNR cell (scale bar 50 μm). **(n)** Light-evoked EPSC recorded in mCherry-positive SNR cell (black) in response to stimulation of LPB inputs (red trace: 20 μM CNQX). **(o)** Mean EPSC amplitude before (ACSF) and after CNQX application. **(p)** eYFP-expressing LPB_{GAD2} neurons at bregma −5.30 mm. **(q-s)** LPB_{GAD2} terminals expressing eYFP in (q) DLPAG (Bregma: −4.60 mm), but not in (r) ventral midbrain (Bregma: −3.30 mm) or (s) amygdala (Bregma: −1.50 mm; scale bar 200 μm). **(t)** Left: Retrobead injection site in NAcLat of a VGLUT2-Cre mouse for experiment in Fig. 1g (scale bar 200 μm). Middle/Right: lVTA cell that was recorded for experiment in Fig. 1g and filled with neurobiotin (NB). It is retrogradely labeled (i.e., projects to NAcLat) and TH-immunopositive (scale bar 50 μm). **(u)** Same as in (t) but cell is in SNR and TH-immunonegative (scale bar 50 μm). **(v)** Recorded VTA cell from a GAD2tdTomato mouse and filled with NB (Refers to Fig. 1k; scale bar 50 μm). Data represent mean ± SEM. Significance was calculated by means of one-way RM ANOVA with Tukey's post-hoc test (k) or paired t-test (o). * $p < 0.05$, ** $p < 0.01$, *** $p < 0.001$.

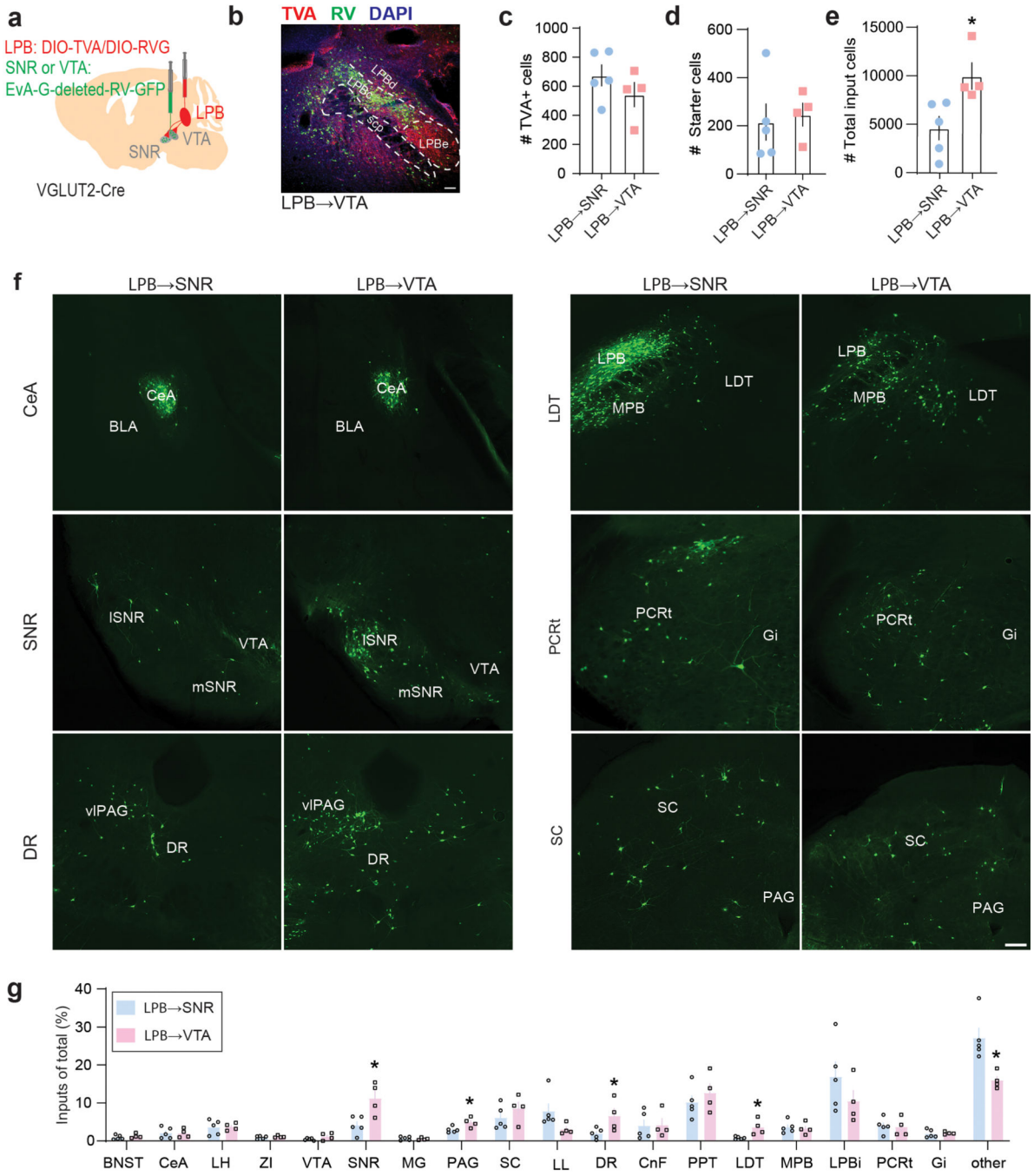

Extended Data Fig. 2. Whole brain mapping of monosynaptic inputs to LPB→SNR and LPB→VTA neurons.

(a) Schematic showing AAV helper virus (DIO-TVA and DIO-RVG) injections into LPB and EvA-RV-GFP into SNR or VTA of VGLUT2-Cre mice. **(b)** Sample coronal brain section showing VTA-projecting starter cells in LPB (green: EnvA-ΔG-GFP; red: TVA-mCherry, blue: DAPI; scale bar 100 μm). **(c)** Bar graph showing quantification of TVA-expressing cells (red) in LPB. **(d)** Bar graph showing number of starter cells in LPB. **(e)** Total number of EnvA-ΔG-GFP labeled cells across all brain regions analyzed. **(f)**

Sample images showing GFP-expressing cells (green) that make monosynaptic inputs onto LPB→SNR or LPB→VTA neurons for different brain areas (scale bar 100 μm). **(g)** Quantification of inputs to LPB→SNR and LPB→VTA neurons. Data are presented as a percentage of total input neurons counted in each individual brain region (BNST: bed nucleus of the stria terminalis, CeA: central nucleus of the amygdala, BLA: basolateral amygdala, LH: lateral hypothalamic area, ZI: zona incerta, VTA: ventral tegmental area, SNR: substantia nigra, reticular part, MG: medial geniculate nucleus, PAG: periaqueductal grey, vlPAG: ventrolateral periaqueductal gray, SC: superior colliculus, LL: lateral lemniscus, DR: dorsal raphe nucleus, CnF: cuneiform nucleus, PPT: pedunculopontine tegmental nucleus, LDT: laterodorsal tegmental nucleus, MPB: medial parabrachial nucleus, LPBi: ipsilateral LPB, PACRt:parvicellular reticular nucleus, Gi: gigantocellular reticular nucleus; n = 4–5 mice). Data represent mean ± SEM. Significance was calculated by means of unpaired t-test. * $p < 0.05$. Comparisons with no asterisk had $p > 0.05$ and were not considered significant.

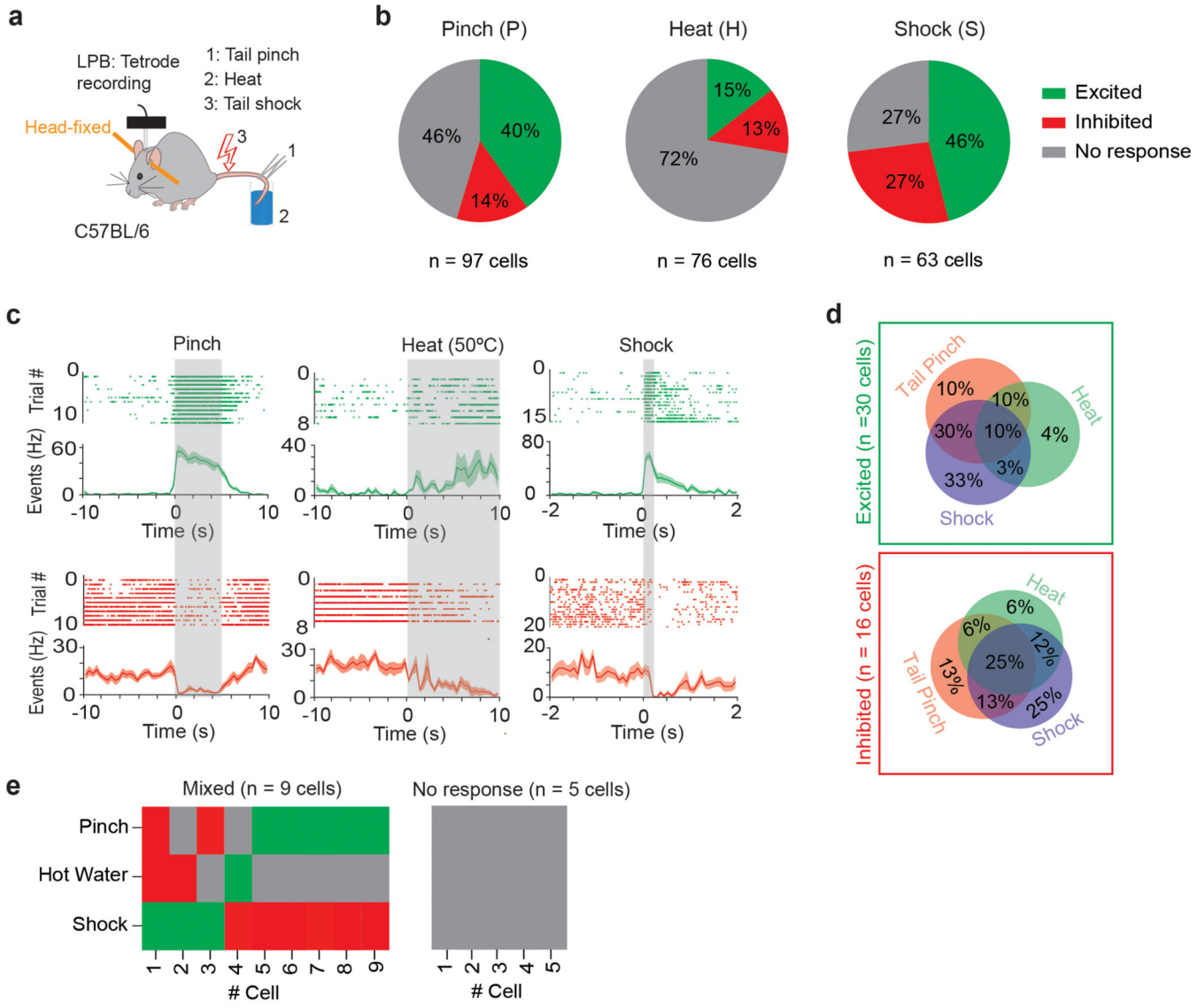

Extended Data Fig. 3. Heterogenous responses to noxious stimuli in LPB neurons.

(a) Schematic of experimental design showing *in vivo* electrophysiological recordings of non-projection defined LPB neurons. Animals were exposed to tail pinch, heat, and electrical shock. **(b)** Pie graphs represent the proportion of LPB cells that are excited (green), inhibited (red) and do not respond (grey) to tail pinch, heat, or electrical tail shock (n = 63–97 cells from n = 5 mice). **(c)** Samples of spike raster plots and firing patterns for two different LPB cells that either excited (top) or inhibited (bottom) in response to noxious stimuli. Note that the top and bottom graphs are from the same LPB cell (i.e., an LPB cell that was excited by all three noxious stimuli (top) and another LPB cell that was inhibited by all three noxious stimuli (bottom)). **(d,e)** Analysis for LPB cells that were recorded in response to all three noxious stimuli (n = 60 cells). Overlap between the proportion of LPB cells that were excited (top, green, n = 30 cells) or inhibited (bottom, red, n = 16 cells) in response to individual noxious stimuli (d) and LPB cells that show both excitatory and

inhibitory responses for individual noxious stimuli (left, n = 9 cells) or did not respond at all (right, n = 5 cells) (e).

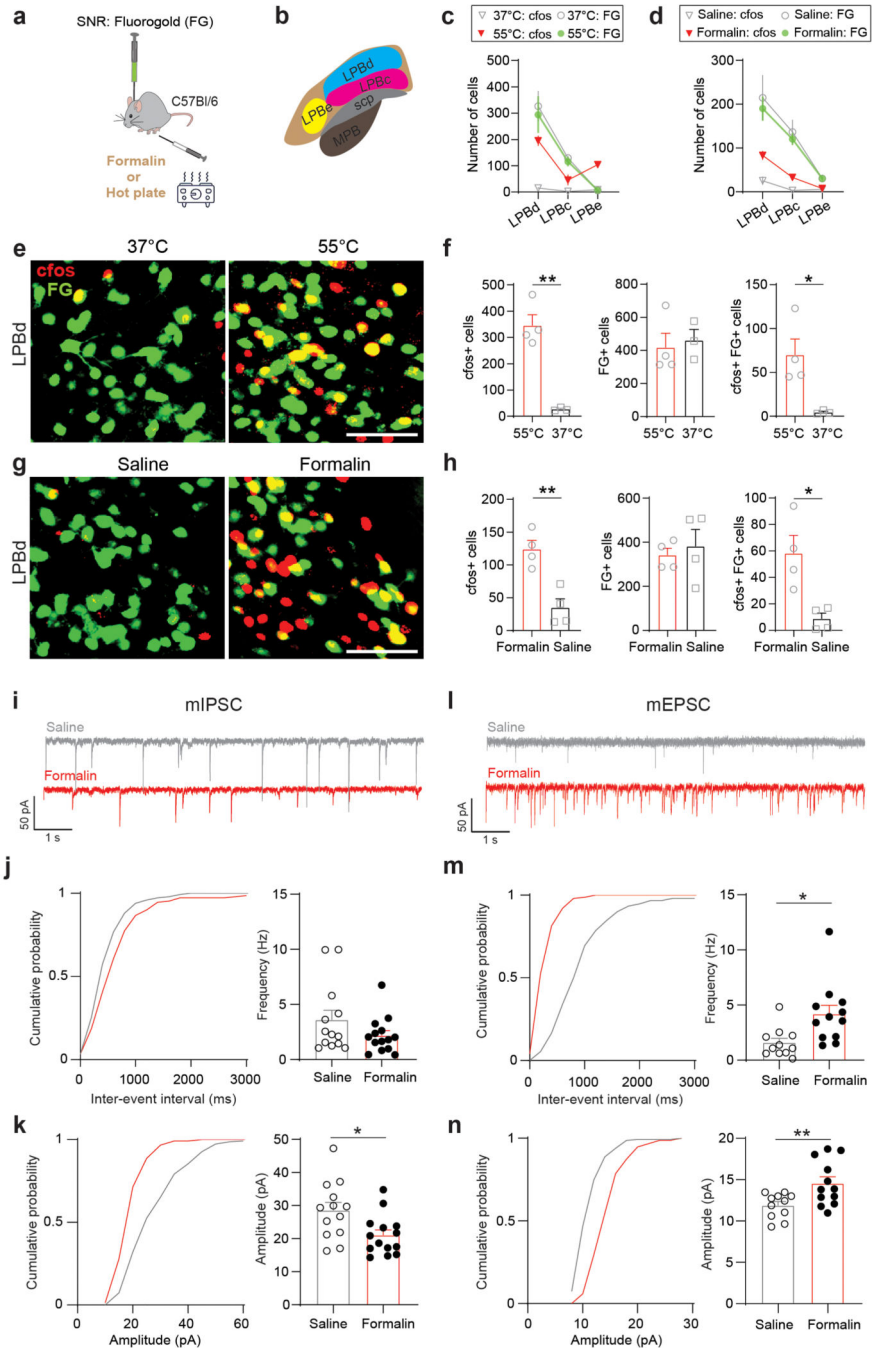

Extended Data Fig. 4. Noxious stimuli activate LPB→SNR neurons and alter excitatory and inhibitory transmission.

(a) Mice were subjected to a hot plate test (c,e,f) or received unilateral intraplantar injection of 1% formalin or saline (d,g,h). **(b)** LPB subregions are highlighted in different colors to demonstrate location of LPB subpopulations projecting to SNR (blue), VTA (red) or CeA (yellow). **(c)** Mean number of c-Fos-immunopositive cells in animals exposed to 37°C

(white triangle) or 55°C (red triangle) heat and mean number of FG labeled cells for each temperature level (white and red circle, respectively) for different LPB subregions described in (b) (37°C: n = 3 mice; 55°C: n = 4 mice). **(d)** Same as in (c), but for animals that received intraplantar injections of 1% formalin or saline (n = 4 mice). **(e)** Retrogradely-labeled SNR-projecting LPB cells (green, FG) and c-Fos immunoreactivity (red) in response to 37°C (left) or 55°C (right) heat (scale bar 50 μm). **(f)** Animals that have been exposed to 55°C heat display significantly increased c-Fos immunoreactivity in LPB cells (left) and in SNR-projecting LPB neurons (right, FG-positive cells) when compared to 37°C heat. No difference in mean number of FG-labeled LPB cells between 37°C and 55°C heat (middle). **(g,h)** Same as in (e,f), but for animals that received intraplantar injections of 1% formalin or saline. **(i-k)** Sample traces of miniature inhibitory postsynaptic currents (mIPSCs) from SNR-projecting LPB neurons recorded from animals that received intraplantar injections of 1% formalin (red) or saline (grey; cells recorded in 1 μM TTX, 20 μM CNQX, 50 μM D-AP5) (i). Cumulative probability plots and bar graphs of the means from the frequencies (j) and amplitudes (k) of mIPSCs recorded from SNR-projecting LPB neurons (saline: n = 13 cells; formalin: n = 14 cells). **(l-n)** Same as in (i-k), but for recordings of miniature excitatory postsynaptic currents (mEPSCs; cells recorded in 1 μM TTX, 100 μM picrotoxin; saline: n = 11 cells; formalin: n = 12 cells). Data represent mean ± SEM. Significance was calculated by means of unpaired t-test for across group comparison (f,h,j,k,m,n). * $p < 0.05$, ** $p < 0.01$.

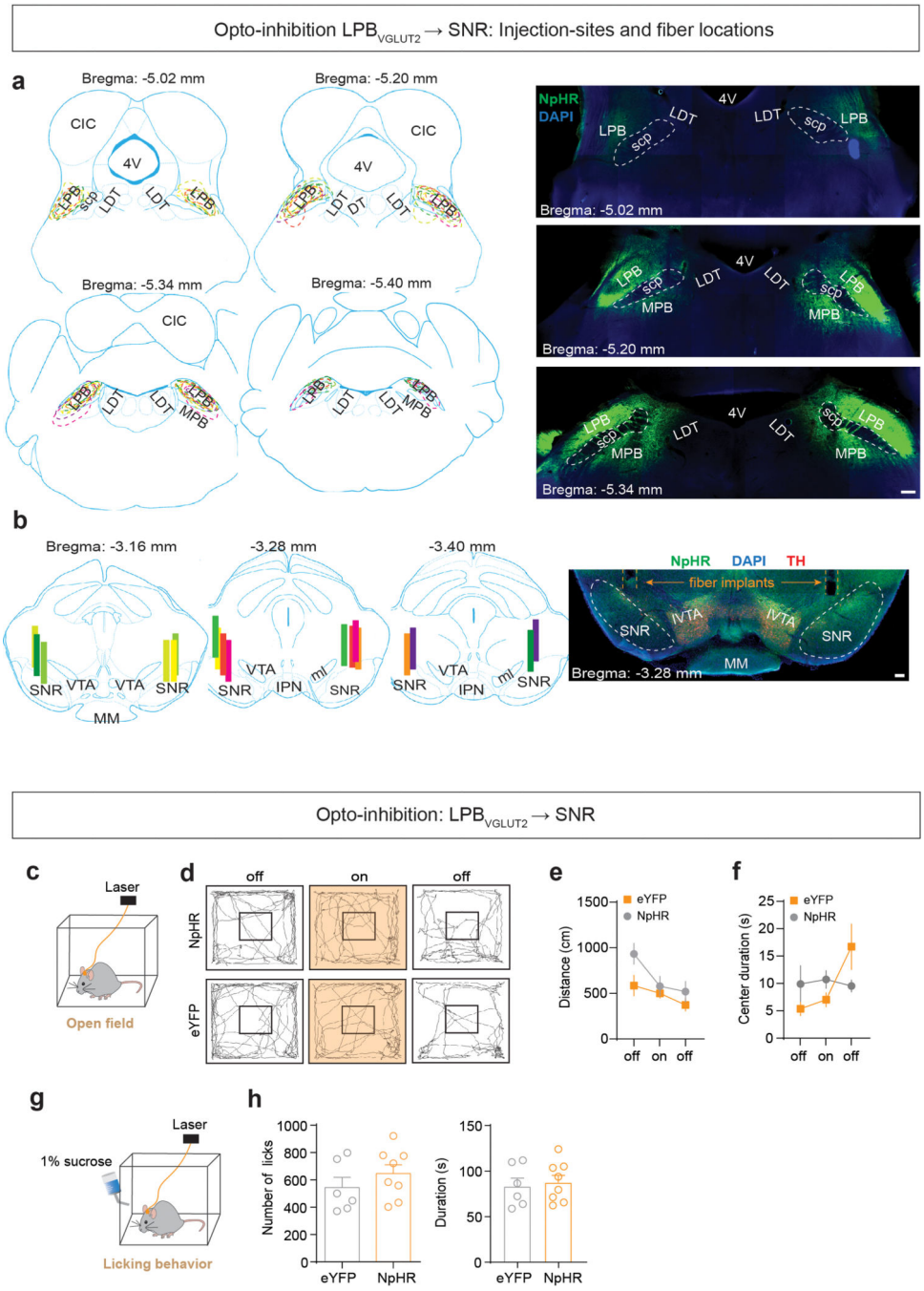

Extended Data Fig. 5. Optogenetic silencing of the LPB→SNR pathway does not affect locomotor activity and general licking behavior.

(a) Serial reconstruction of viral injection sites in LPB. Right panels show representative examples of NpHR-eYFP (green) injection sites across the rostro-caudal extent of the LPB (scale bar 100 μm). Left panels show schematics of the corresponding brain regions in which NpHR-eYFP was detected. Each color represents the expression profile from a single mouse that was used for the experiments shown in **Fig. 4a–f**. **(b)** Corresponding serial reconstructions of optical fiber locations in the SNR (TH: red; scale bar 100 μm).

(c) Schematic design of open field test for assessing the effects of optogenetic silencing of the LPB→SNR pathway on general locomotor activity. **(d)** Representative trajectories of animals expressing NpHR (top) or eYFP (bottom). **(e,f)** Optogenetic silencing of the LPB→SNR pathway does not have a significant effect on the (e) mean distance traveled (a measure for locomotor activity) or (f) time spent in the center of the box in NpHR- (n = 9 mice) and eYFP-expressing (n = 5 mice) mice. **(g)** Schematic showing control experiment for studying general licking behavior in response to optogenetic silencing of LPB→SNR neurons. **(h)** Bar graphs showing mean number (left) and duration (right) of licks for sucrose solution in NpHR- (n = 8 mice) and eYFP-expressing (n = 6 mice) mice. Data represent mean ± SEM. Significance was calculated by means of one-way RM ANOVA with Tukey's post-hoc test (e,f) or unpaired t-test (h). Comparisons with no asterisk had $p > 0.05$ and were not considered significant.

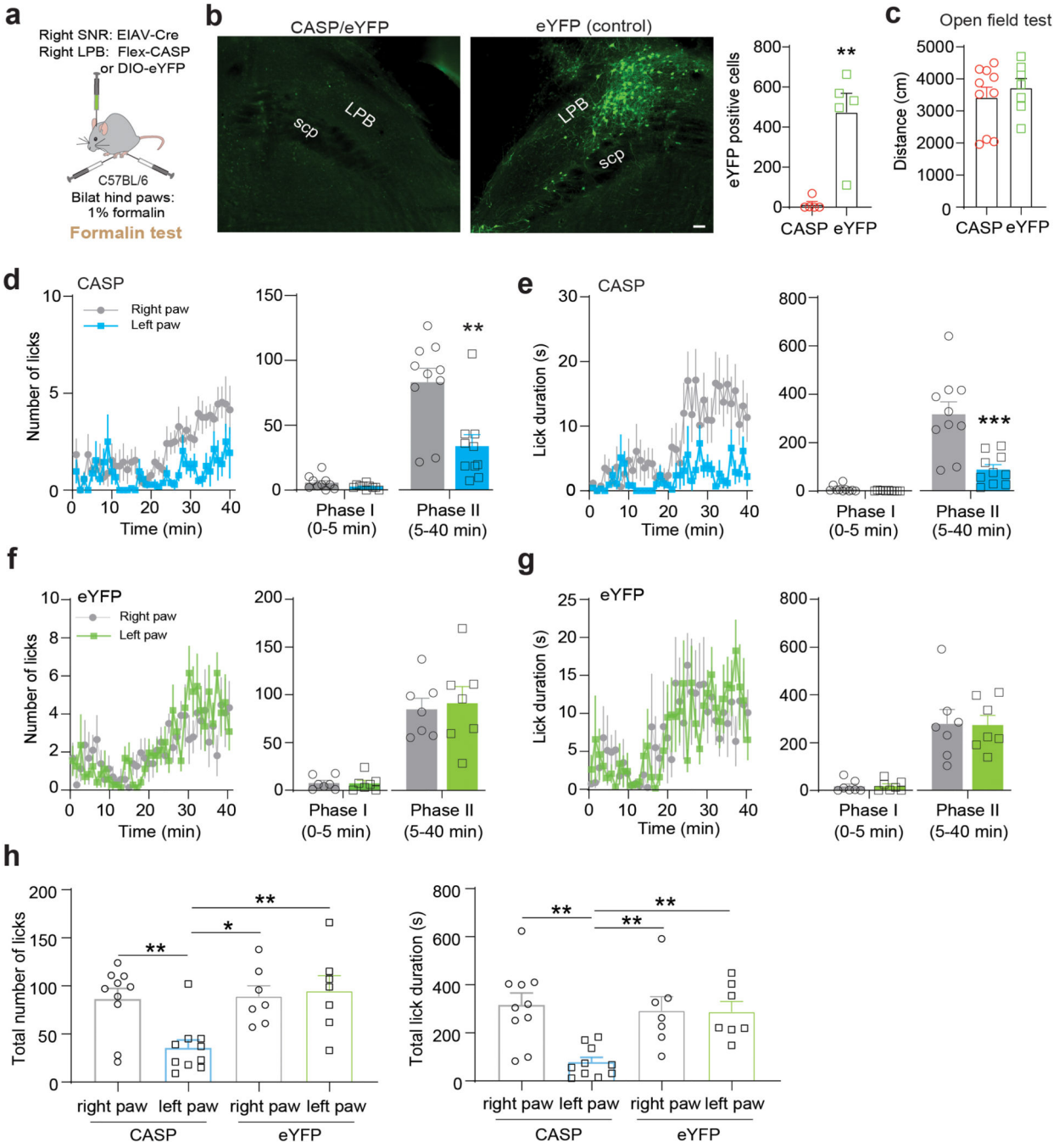

Extended Data Fig. 6. Genetic ablation of LPB→SNR neurons reduces behavioral responses to formalin-induced pain.

(a) Injection of retrogradely-transported pseudotyped equine infectious anemia virus expressing Cre-recombinase (RG-EIAVCre) into the right SNR and AAV carrying Cre-dependent Caspase 3 (CASP) or eYFP into the right LPB of C57BL/6 mice. 5 weeks later, mice received bilateral intraplantar injections of 1% formalin into the hind paws. **(b)** Comparison between animals in which SNR-projecting LPB neurons were genetically ablated using CASP (left) and animals that express a control vector (eYFP) in SNR-

projecting LPB neurons (middle). Sections were stained using an eYFP antibody (green; scale bar 50 μm). CASP animals show significantly reduced number of eYFP-positive SNR-projecting LPB cells when compared to control animals (right; CASP: n = 5 mice, eYFP: n = 5 mice). **(c)** Mean total distance traveled was not significantly different between CASP and eYFP animals in the open field test (CASP: n = 10 mice, eYFP: n = 7 mice). **(d)** Number of licks in response to formalin injection in CASP mice (n = 10 mice) for the left (blue) and right (grey) hind paws (left). Mean number of licks during phase I and phase II of the formalin test for comparison of left and right hind paws (right). **(e)** Same as in (d) but for analysis of lick duration. **(f,g)** Same as in (d,e) but for eYFP control animals (n = 7 mice). **(h)** Comparison of mean total number of licks (left) and mean total lick duration (right) for CASP and eYFP mice for individual hind paws. Data represent mean ± SEM. Significance was calculated by means of unpaired t-test (a,b,d,e,f,g) and one-way RM ANOVA with Tukey's post-hoc test (h). * $p < 0.05$, ** $p < 0.01$, *** $p < 0.001$.

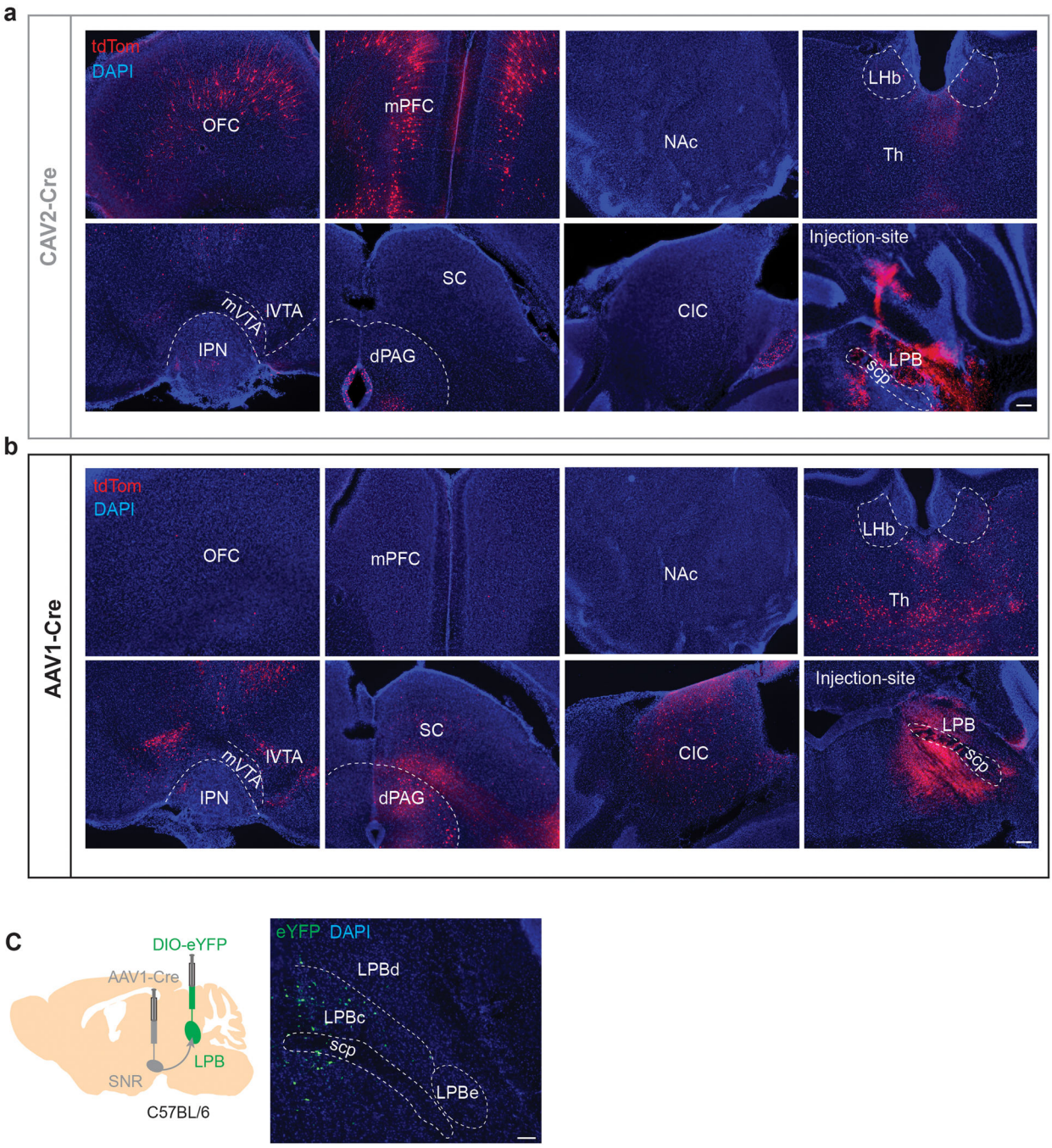

Extended Data Fig. 7. Comparison of transsynaptic distribution of AAV1-Cre versus CAV2-Cre.
(a,b) Sample fluorescent images showing tdTomato labeled neurons (red) in different brain regions in response to (a) CAV2-Cre or (b) AAV1-Cre injection into the LPB of Ai14 mice (n = 2 mice for each condition) (DAPI: blue; scale bars 100 μm). **(c)** Left: Schematic showing injection of AAV1-Cre into SNR and AAV-DIO-eYFP into LPB of C57BL/6 mice (n = 2 mice). Right: Sample fluorescent image showing that eYFP-expressing cells are predominantly located in the LPBc (DAPI: blue; scale bar 100 μm).

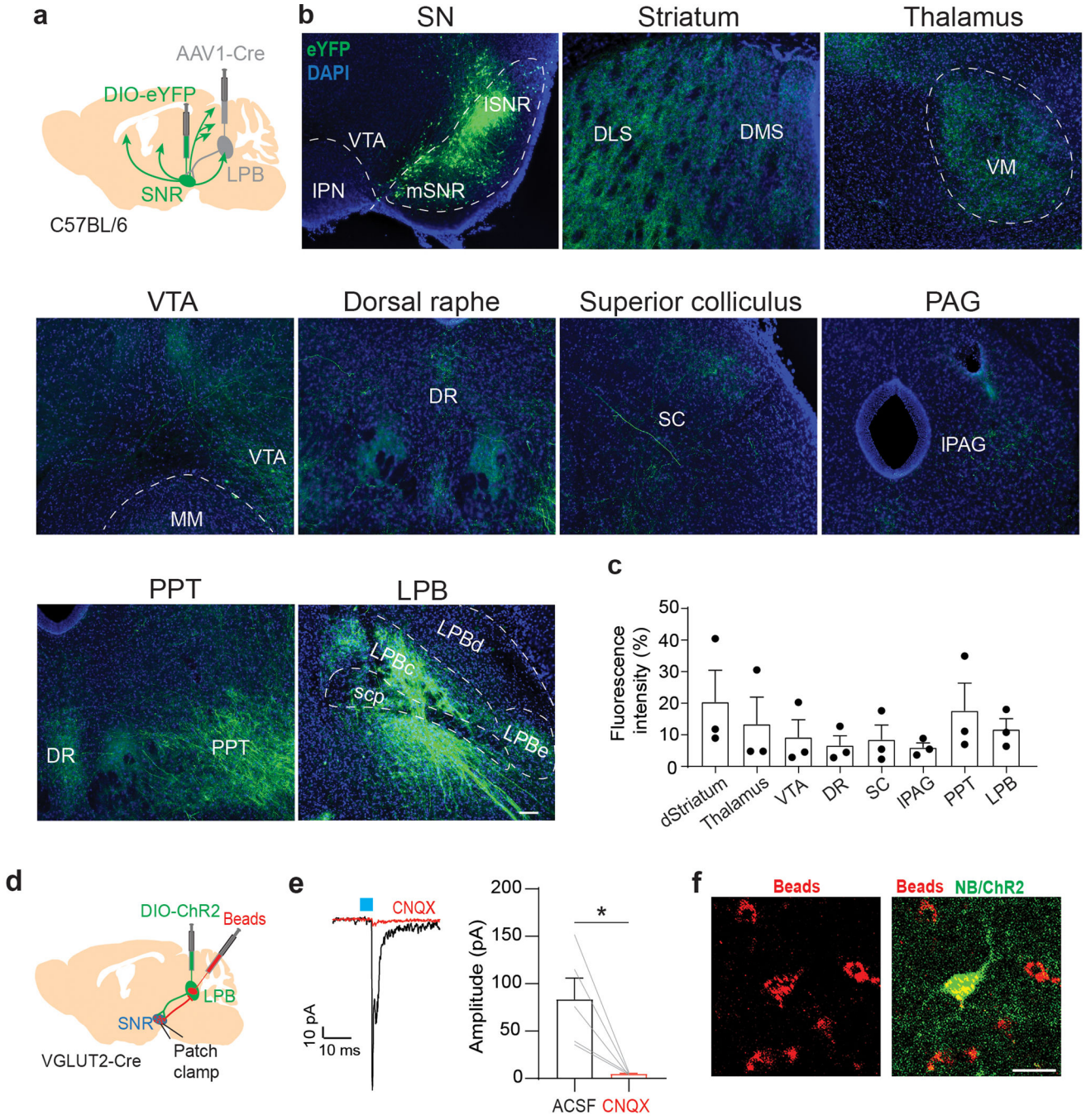

Extended Data Fig 8. Whole-brain projections of LPB-targeted SNR neurons.

(a) Schematic showing unilateral targeting of anterogradely-transported AAV1-Cre to LPB and AAV carrying Cre-dependent eYFP to SNR of C57BL/6 mice. **(b)** Representative fluorescent images showing coronal brain sections of eYFP-expressing cells in the SNR (upper left image) and eYFP-expressing terminals across different brain regions (scale bar 100 μm). **(c)** Quantification of fluorescence intensity of eYFP-expressing terminals in different brain regions (n = 3 mice). **(d)** Schematic showing injection of fluorescent retrobeads and AAV-DIO-ChR2 into the LPB of VGLUT2-Cre mice. Whole-cell patch-

clamp recordings were performed from retrogradely-labeled (i.e., beads-positive) cells in the lateral SNR. **(e)** Left: Sample trace showing light-evoked EPSC from LPB-projecting SNR neurons (black trace) in response to light stimulation of LPB inputs. Light-evoked EPSCs are blocked by bath application of 20 μM CNQX (red trace). Right: Bar graph showing mean EPSC amplitudes before (ACSF) and after bath application of CNQX (n = 5 cells). **(f)** Sample image of retrogradely-labeled (beads, red) cells in the lateral SNR that were filled with neurobiotin (NB, green) during whole-cell patch-clamp recordings (scale bar 50 μm). Significance was calculated by means of paired t-test (e). * $p < 0.05$. Data represent mean ± SEM.

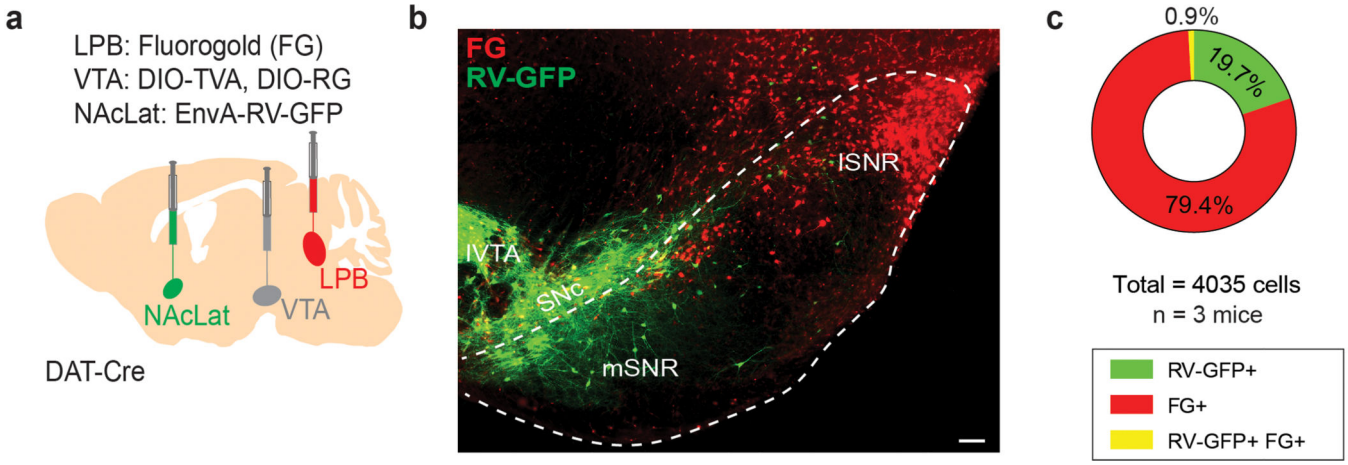

Extended Data Fig. 9. SNR→LPB neurons have very few collaterals to NAcLat-projecting VTA DA neurons.

(a) Schematic showing injection of fluorogold (FG) into the LPB and AAVs encoding the cellular receptor for subgroup A avian leukosis viruses (TVA) and rabies virus glycoprotein (RG) in the VTA of DAT-Cre mice. In the same animals, EnvA-pseudotyped, glycoprotein-deficient rabies virus expressing GFP (EnvA-RV-GFP) was targeted to the NAcLat. **(b)** Representative example of coronal section of the ventral midbrain showing retrogradely-labeled cells in the lateral SNR (i.e., LPB-projecting, FG-positive, red). GFP-positive cells (green) make monosynaptic connections onto VTA DA neurons projecting to NAcLat and are mainly located in the substantia nigra pars compacta (SNc), ventral SNR (vSNR) and lateral VTA, but do not overlap with the lateral SNR (lSNR; scale bar 100 μm). **(c)** Pie chart showing proportion of analyzed cells (n = 4035 cells from n = 3 mice) in the ventral midbrain that express GFP (green, 19.7%) or are labeled by FG (red, 79.4%) or contain both GFP and FG (yellow, 0.9%).

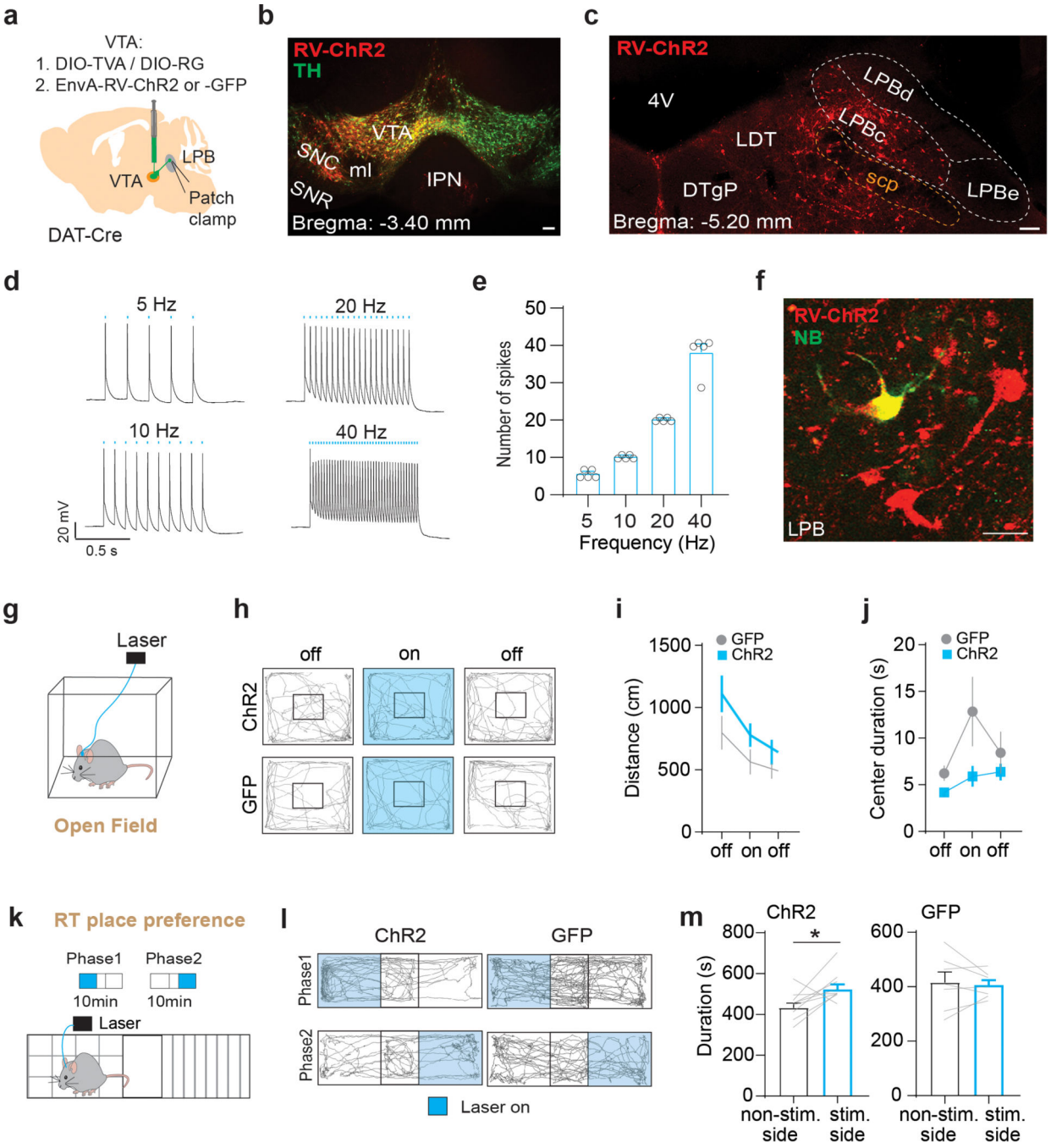

Extended Data Fig. 10. Optogenetic stimulation of LPB→VTA DA neurons does not affect locomotor activity but promotes reward-related behavior.

(a) Targeting of AAVs encoding the cellular receptor for subgroup A avian leukosis viruses (TVA) and rabies virus glycoprotein (RG) as well as EnvA-pseudotyped, glycoprotein-deficient rabies virus expressing ChR2 or GFP (EnvA-RV-ChR2/-GFP) to VTA of DAT-Cre mice. Patch-clamp recordings were performed from LPB neurons (d-f) or bilateral optical fibers were implanted above the LPB for assessment of locomotor activity in open field test (g-j). **(b)** Injection site in VTA (scale bar 100 μm). **(c)** ChR2-expressing cells in LPB,

which make monosynaptic connections onto VTA DA neurons (scale bar 100 μm). **(d)** Sample patch-clamp recordings from LPB neurons showing light-evoked action potentials in response to 5 Hz, 10 Hz, 20 Hz or 40 Hz stimulation (scale bars 20 mV/0.5 sec). **(e)** Mean number of spikes in response to different stimulation frequencies (5 Hz: n = 5 cells, 10 Hz: n = 5 cells, 20 Hz: n = 5 cells, 40 Hz: n = 5 cells). **(f)** Neurobiotin (NB)-filled LPB cell expressing ChR2 (scale bar 20 μm). **(g)** Experimental design. **(h)** Representative trajectories of animals expressing ChR2 (top) or GFP (bottom) in LPB→VTA DA neurons. **(i)** 20 Hz stimulation of LPB→VTA DA neurons does not have significant effect on the mean distance traveled between ChR2- (left) and GFP-expressing (right) mice. **(j)** No significant difference in time spent in center area between ChR2 and GFP mice. **(k)** Schematic of real-time (RT) place preference assay. **(l)** Trajectories of sample ChR2- and GFP-expressing mice during RT place preference test. **(m)** ChR2- (left) but not GFP-expressing (right) mice spent significantly more time on the side of the chamber paired with light stimulation of LPB→VTA DA neurons (ChR2: n = 9 mice, GFP: n = 7 mice). Data represent mean ± SEM. Significance was calculated by means of one-way RM ANOVA with Tukey's post-hoc test (i) and two-way RM ANOVA with Holm-Sidak's post-hoc test (j) or paired t-tests (m). * $p < 0.05$.

Supplementary Material

Refer to Web version on PubMed Central for supplementary material.

ACKNOWLEDGEMENTS

S.L. is a Weill Neurohub Investigator, John P. Stock Faculty Fellow and Rita Allen Scholar. This work was supported by NIH (R01DA042889, S.L.; R01MH107742, B.K.L; U01MH114829, B.K.L), NARSAD Young Investigator Award (23543, S.L.), Brain Research Foundation (BRFSG-2015-7, S.L.), Wayne and Gladys Valley Foundation (S.L.), One Mind Foundation (S.L.) and National Natural Science Foundation of China (61721092, 61890953, H.G.). The funders had no role in study design, data collection and analysis, decision to publish or preparation of the manuscript. We thank Dr. Jochen Roeper (Goethe University) for critical reading of the manuscript.

REFERENCES

1. Berridge KC & Kringelbach ML Pleasure Systems in the Brain. Neuron 86, 646–664 (2015). [PubMed: 25950633]
2. Schultz W. Dopamine reward prediction-error signalling: a two-component response. Nat. Rev. Neurosci. 17, 183 (2016). [PubMed: 26865020]
3. Watabe-Uchida M, Eshel N. & Uchida N. Neural Circuitry of Reward Prediction Error. Annu. Rev. Neurosci. 40, 373–394 (2017). [PubMed: 28441114]
4. Wise RA & Rompre PP Brain dopamine and reward. Annu Rev Psychol 40, 191–225 (1989). [PubMed: 2648975]
5. Borsook D. et al. Reward deficiency and anti-reward in pain chronification. Neurosci. Biobehav. Rev. 68, 282–297 (2016). [PubMed: 27246519]
6. Porreca F. & Navratilova E. Reward, motivation, and emotion of pain and its relief: PAIN 158, S43–S49 (2017). [PubMed: 28106670]
7. Taylor AMW, Becker S, Schweinhardt P. & Cahill C. Mesolimbic dopamine signaling in acute and chronic pain: implications for motivation, analgesia, and addiction. PAIN 157, 1194–1198 (2016). [PubMed: 26797678]
8. Wood PB Role of central dopamine in pain and analgesia. Expert Rev. Neurother. 8, 781–797 (2008). [PubMed: 18457535]

9. Coizet V, Dommett EJ, Klop EM, Redgrave P. & Overton PG The parabrachial nucleus is a critical link in the transmission of short latency nociceptive information to midbrain dopaminergic neurons. Neuroscience 168, 263–272 (2010). [PubMed: 20363297]
10. de Jong JW et al. A Neural Circuit Mechanism for Encoding Aversive Stimuli in the Mesolimbic Dopamine System. Neuron 101, 133–151.e7 (2019). [PubMed: 30503173]
11. Maeda H. & Mogenson GJ Effects of peripheral stimulation on the activity of neurons in the ventral tegmental area, substantia nigra and midbrain reticular formation of rats. Brain Res. Bull. 8, 7–14 (1982). [PubMed: 7055735]
12. Mirenowicz J. & Schultz W. Preferential activation of midbrain dopamine neurons by appetitive rather than aversive stimuli. Nature 379, 449–51 (1996). [PubMed: 8559249]
13. Ungless MA Uniform Inhibition of Dopamine Neurons in the Ventral Tegmental Area by Aversive Stimuli. Science 303, 2040–2042 (2004). [PubMed: 15044807]
14. Navratilova E. et al. Pain relief produces negative reinforcement through activation of mesolimbic reward-valuation circuitry. Proc. Natl. Acad. Sci. 109, 20709–20713 (2012). [PubMed: 23184995]
15. Defazio G. et al. Pain as a nonmotor symptom of Parkinson disease: evidence from a case-control study. Arch. Neurol. 65, 1191–1194 (2008). [PubMed: 18779422]
16. Huang S, Borgland SL & Zamponi GW Peripheral nerve injury-induced alterations in VTA neuron firing properties. Mol. Brain 12, (2019).
17. Ren W. et al. Adaptive alterations in the mesoaccumbal network following peripheral nerve injury. Pain (2020) doi:10.1097/j.pain.0000000000002092.
18. Schwartz N. et al. Decreased motivation during chronic pain requires long-term depression in the nucleus accumbens. Science 345, 535–542 (2014). [PubMed: 25082697]
19. Finan PH & Smith MT The comorbidity of insomnia, chronic pain, and depression: dopamine as a putative mechanism. Sleep Med. Rev. 17, 173–183 (2013). [PubMed: 22748562]
20. Cechetto DF, Standaert DG & Saper CB Spinal and trigeminal dorsal horn projections to the parabrachial nucleus in the rat. J. Comp. Neurol. 240, 153–160 (1985). [PubMed: 3840498]
21. Deng J. et al. The Parabrachial Nucleus Directly Channels Spinal Nociceptive Signals to the Intralaminar Thalamic Nuclei, but Not the Amygdala. Neuron 107, 909–923.e6 (2020). [PubMed: 32649865]
22. Gauriau C. & Bernard J-F Pain Pathways and Parabrachial Circuits in the Rat. Exp. Physiol. 87, 251–258 (2002). [PubMed: 11856971]
23. Bernard JF, Huang GF & Besson JM The parabrachial area: electrophysiological evidence for an involvement in visceral nociceptive processes. J. Neurophysiol. 71, 1646–1660 (1994). [PubMed: 8064340]
24. Campos CA, Bowen AJ, Roman CW & Palmiter RD Encoding of danger by parabrachial CGRP neurons. Nature 555, 617–622 (2018). [PubMed: 29562230]
25. Bernard JF, Bester H. & Besson JM Chapter 14 Involvement of the spino-parabrachio -amygdaloid and -hypothalamic pathways in the autonomic and affective emotional aspects of pain. in Progress in Brain Research vol. 107 243–255 (Elsevier, 1996). [PubMed: 8782523]
26. Chiang MC et al. Divergent Neural Pathways Emanating from the Lateral Parabrachial Nucleus Mediate Distinct Components of the Pain Response. Neuron 106, 927–939.e5 (2020). [PubMed: 32289251]
27. Han S, Soleiman MT, Soden ME, Zweifel LS & Palmiter RD Elucidating an Affective Pain Circuit that Creates a Threat Memory. Cell 162, 363–374 (2015). [PubMed: 26186190]
28. Palmiter RD The Parabrachial Nucleus: CGRP Neurons Function as a General Alarm. Trends Neurosci. 41, 280–293 (2018). [PubMed: 29703377]
29. Saper CB & Loewy AD Efferent connections of the parabrachial nucleus in the rat. Brain Res. 197, 291–317 (1980). [PubMed: 7407557]
30. Morales M. & Margolis EB Ventral tegmental area: cellular heterogeneity, connectivity and behaviour. Nat. Rev. Neurosci. 18, 73–85 (2017). [PubMed: 28053327]
31. Yang H. et al. Nucleus Accumbens Subnuclei Regulate Motivated Behavior via Direct Inhibition and Disinhibition of VTA Dopamine Subpopulations. Neuron 97, 434–449.e4 (2018). [PubMed: 29307710]

32. Barrot M. Tests and models of nociception and pain in rodents. Neuroscience 211, 39–50 (2012). [PubMed: 22244975]
33. Magarinos-Ascone C, García-Austt E. & Buño W. Polymodal sensory and motor convergence in substantia nigra neurons of the awake monkey. Brain Res. 646, 299–302 (1994). [PubMed: 8069677]
34. Mailly P, Charpier S, Menetrey A. & Deniau J-M Three-Dimensional Organization of the Recurrent Axon Collateral Network of the Substantia Nigra Pars Reticulata Neurons in the Rat. J. Neurosci. 23, 5247–5257 (2003). [PubMed: 12832549]
35. Abbott FV, Franklin KB & Westbrook RF The formalin test: scoring properties of the first and second phases of the pain response in rats. Pain 60, 91–102 (1995). [PubMed: 7715946]
36. Rossi MA et al. A GABAergic nigrotectal pathway for coordination of drinking behavior. Nat. Neurosci. 19, 742–748 (2016). [PubMed: 27043290]
37. Johansen JP & Fields HL Glutamatergic activation of anterior cingulate cortex produces an aversive teaching signal. Nat. Neurosci. 7, 398–403 (2004). [PubMed: 15004562]
38. Häusser M. Optogenetics: the age of light. Nat. Methods 11, 1012–1014 (2014). [PubMed: 25264778]
39. Yang CF et al. Sexually dimorphic neurons in the ventromedial hypothalamus govern mating in both sexes and aggression in males. Cell 153, 896–909 (2013). [PubMed: 23663785]
40. Patriarchi T. et al. Ultrafast neuronal imaging of dopamine dynamics with designed genetically encoded sensors. Science 360, (2018).
41. Bernard JF, Huang GF & Besson JM The parabrachial area: electrophysiological evidence for an involvement in visceral nociceptive processes. J. Neurophysiol. 71, 1646–1660 (1994). [PubMed: 8064340]
42. Han W. et al. A Neural Circuit for Gut-Induced Reward. Cell 175, 665–678.e23 (2018). [PubMed: 30245012]
43. Fernandes AB et al. Postingestive Modulation of Food Seeking Depends on Vagus-Mediated Dopamine Neuron Activity. Neuron 106, 778–788.e6 (2020). [PubMed: 32259476]
44. Matsumoto M. & Hikosaka O. Two types of dopamine neuron distinctly convey positive and negative motivational signals. Nature 459, 837–841 (2009). [PubMed: 19448610]
45. Lammel S. et al. Input-specific control of reward and aversion in the ventral tegmental area. Nature 491, 212–217 (2012). [PubMed: 23064228]
46. Stamatakis AM & Stuber GD Activation of lateral habenula inputs to the ventral midbrain promotes behavioral avoidance. Nat Neurosci 15, 1105–7 (2012). [PubMed: 22729176]
47. Gao DM, Jeaugey L, Pollak P. & Benabid AL Intensity-dependent nociceptive responses from presumed dopaminergic neurons of the substantia nigra, pars compacta in the rat and their modification by lateral habenula inputs. Brain Res. 529, 315–319 (1990). [PubMed: 2282499]
48. Tian J. & Uchida N. Habenula Lesions Reveal that Multiple Mechanisms Underlie Dopamine Prediction Errors. Neuron 87, 1304–1316 (2015). [PubMed: 26365765]
49. Brown MT, Henny P, Bolam JP & Magill PJ Activity of neurochemically heterogeneous dopaminergic neurons in the substantia nigra during spontaneous and driven changes in brain state. J Neurosci 29, 2915–25 (2009). [PubMed: 19261887]
50. Henny P. et al. Structural correlates of heterogeneous in vivo activity of midbrain dopaminergic neurons. Nat. Neurosci. 15, 613–619 (2012). [PubMed: 22327472]
51. Lerner TN et al. Intact-Brain Analyses Reveal Distinct Information Carried by SNc Dopamine Subcircuits. Cell 162, 635–647 (2015). [PubMed: 26232229]
52. Brischoux F, Chakraborty S, Brierley DI & Ungless MA Phasic excitation of dopamine neurons in ventral VTA by noxious stimuli. Proc. Natl. Acad. Sci. 106, 4894–4899 (2009). [PubMed: 19261850]
53. Hikosaka O. & Wurtz RH Visual and oculomotor functions of monkey substantia nigra pars reticulata. IV. Relation of substantia nigra to superior colliculus. J. Neurophysiol. 49, 1285–1301 (1983). [PubMed: 6306173]
54. Liu D. et al. A common hub for sleep and motor control in the substantia nigra. Science 367, 440–445 (2020). [PubMed: 31974254]

55. Brown J, Pan W-X & Dudman JT The inhibitory microcircuit of the substantia nigra provides feedback gain control of the basal ganglia output. eLife 3, e02397 (2014).
56. Deniau JM & Chevalier G. The lamellar organization of the rat substantia nigra pars reticulata: Distribution of projection neurons. Neuroscience 46, 361–377 (1992). [PubMed: 1542412]
57. Wang S. & Redgrave P. Microinjections of muscimol into lateral superior colliculus disrupt orienting and oral movements in the formalin model of pain. Neuroscience 81, 967–988 (1997). [PubMed: 9330360]
58. Corder G. et al. An amygdalar neural ensemble that encodes the unpleasantness of pain. Science 363, 276–281 (2019). [PubMed: 30655440]
59. Jääskeläinen SK et al. Role of the dopaminergic system in chronic pain -- a fluorodopa-PET study. Pain 90, 257–260 (2001). [PubMed: 11207397]
60. Jarcho JM, Mayer EA, Jiang ZK, Feier NA & London ED Pain, affective symptoms, and cognitive deficits in patients with cerebral dopamine dysfunction. Pain 153, 744–754 (2012). [PubMed: 22386471]
61. Jhou TC, Fields HL, Baxter MG, Saper CB & Holland PC The Rostromedial Tegmental Nucleus (RMTg), a GABAergic Afferent to Midbrain Dopamine Neurons, Encodes Aversive Stimuli and Inhibits Motor Responses. Neuron 61, 786–800 (2009). [PubMed: 19285474]
62. Beyeler A. et al. Divergent Routing of Positive and Negative Information from the Amygdala during Memory Retrieval. Neuron 90, 348–361 (2016). [PubMed: 27041499]
63. Zhang S-J et al. Optogenetic dissection of entorhinal-hippocampal functional connectivity. Science 340, 1232627 (2013).
64. Kim CK et al. Simultaneous fast measurement of circuit dynamics at multiple sites across the mammalian brain. Nat. Methods 13, 325–328 (2016). [PubMed: 26878381]
65. Tye KM et al. Amygdala circuitry mediating reversible and bidirectional control of anxiety. Nature 471, 358–62 (2011). [PubMed: 21389985]
66. Rosland JH, Tjølsen A, Maehle B. & Hole K. The formalin test in mice: effect of formalin concentration. Pain 42, 235–242 (1990). [PubMed: 2247320]
67. Dubuisson D. & Dennis SG The formalin test: a quantitative study of the analgesic effects of morphine, meperidine, and brain stem stimulation in rats and cats. Pain 4, 161–174 (1977). [PubMed: 564014]
68. Tjølsen A, Berge OG, Hunskaar S, Rosland JH & Hole K. The formalin test: an evaluation of the method. Pain 51, 5–17 (1992). [PubMed: 1454405]
69. Deuis JR, Dvorakova LS & Vetter I. Methods Used to Evaluate Pain Behaviors in Rodents. Front. Mol. Neurosci. 10, (2017).
70. Chaplan SR, Bach FW, Pogrel JW, Chung JM & Yaksh TL Quantitative assessment of tactile allodynia in the rat paw. J. Neurosci. Methods 53, 55–63 (1994). [PubMed: 7990513]
71. Yang H-B et al. cAMP-dependent protein kinase activated Fyn in spinal dorsal horn to regulate NMDA receptor function during inflammatory pain. J. Neurochem. 116, 93–104 (2011). [PubMed: 21054385]
72. Gong H. et al. High-throughput dual-colour precision imaging for brain-wide connectome with cytoarchitectonic landmarks at the cellular level. Nat. Commun. 7, (2016).
73. Osakada F. & Callaway EM Design and generation of recombinant rabies virus vectors. Nat. Protoc. 8, 1583–1601 (2013). [PubMed: 23887178]
74. Lammel S. et al. Unique properties of mesoprefrontal neurons within a dual mesocorticolimbic dopamine system. Neuron 5s7, 760–73 (2008).

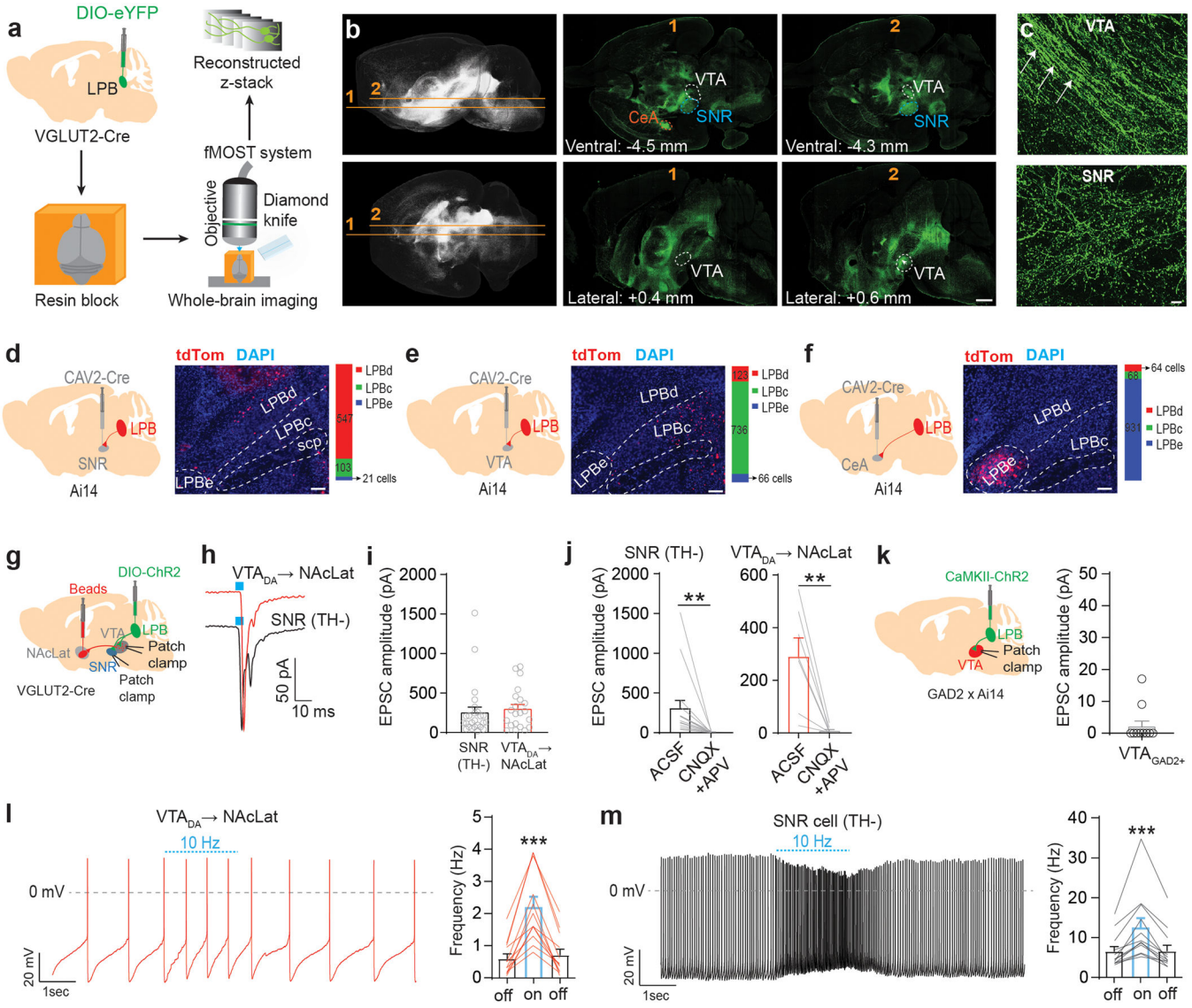

Fig. 1. Functional neuroanatomy of LPB projections to the ventral midbrain.

(a) Experimental design. **(b)** Whole brain fluorescent image showing LPB_{VGLUT2} projections (eYFP = green; upper row: horizontal; lower row: sagittal). VTA, SNR and CeA are highlighted in different colors (scale bar 1 mm). **(c)** LPB_{VGLUT2} terminals and fibers of passage (white arrows) in different ventral midbrain subregions (scale bar 50 μm). **(d-f)** Left: CAV2-Cre injection into (d) SNR, (e) VTA and (f) CeA of Ai14 mice (n = 3 mice for each projection target). Middle: Retrogradely labeled (tdTomato-positive, red) neurons in different LPB subregions (DAPI: blue; scale bars 100 μm). Right: Quantification of retrogradely labeled cells for different LPB subregions (LPBd: lateral parabrachial nucleus - dorsal part; LPBc: lateral parabrachial nucleus - central part; LPBe: lateral parabrachial nucleus – external part). **(g)** Experimental design. **(h)** EPSCs generated at −70 mV by light stimulation of LPB_{VGLUT2} inputs to retrogradely-labeled VTA DA (i.e., TH-immunopositive; Extended Data Fig. 1t) neurons projecting to NAcLat (red trace) or non-DA (i.e., TH-immunonegative; Extended Data Fig. 1u) cells in the SNR (black trace).

(i) Mean EPSC amplitudes produced by light stimulation of LPB_{VGLUT2} inputs to different cell populations (DA→NAcLat: n = 21 cells; SNR: n = 25 cells; recorded in ACSF). **(j)** Application of 20 μM CNQX and 50 μM APV blocks EPSCs in SNR cells (n = 16 cells) (left) and NAcLat-projecting DA neurons (n = 7 cells) (right). **(k)** Experimental design (left) and EPSC amplitudes produced by light stimulation of excitatory LPB inputs onto GAD2-tdTomato-positive VTA neurons (right, VTA_{GAD2+}, n = 10 cells; recorded in ACSF; Extended Data Fig. 1v). **(l,m)** Spontaneous firing from (l) NAcLat-projecting VTA DA neurons and (m) SNR cells in response to 10 Hz light stimulation of LPB_{VGLUT2} inputs. LPB_{VGLUT2} stimulation significantly increases firing of both NAcLat-projecting DA neurons and SNR cells (NAcLat: n = 12 cells; SNR: n = 12 cells). Significance was calculated by means of paired *t*-test within group comparison (j), unpaired t-test (i) or one-way RM ANOVA test with Tukey's post-hoc test (l,m). ** $p < 0.01$, *** $p < 0.001$. Data represent mean ± SEM.

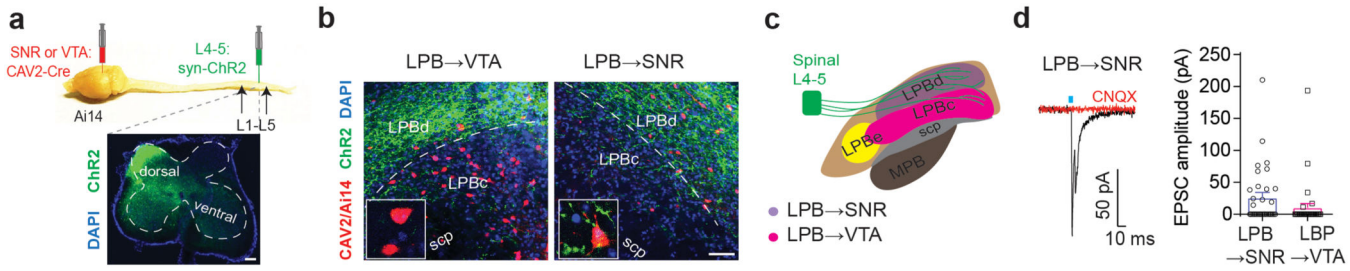

Fig. 2. Spinal cord, dorsal horn neurons target LPB→SNR neurons

(a) Overview showing viral injection of CAV2-Cre into the VTA or SNR and ChR2 (green) into the dorsal horn (lower image) of the spinal cord (L4-L5) of Ai14 mice (DAPI: blue; scale bar 100 μm). **(b)** ChR2-expressing terminals from the dorsal horn (green) are more frequently detected in the LPBd adjacent to retrogradely labeled (tdTomato-positive, red) cells projecting to SNR (right image) than in the LPBc, which contains mainly retrogradely labeled (tdTomato-positive, red) cells projecting to VTA (left image; DAPI: blue; scp: superior cerebellar peduncle; scale bar 50 μm). Insets show higher magnification images of LPB→VTA and LPB→SNR neurons in the LPBc and LPBd, respectively. **(c)** Schematic showing dorsal horn spinal cord projections to different LPB subregions, which are highlighted in different colors to demonstrate the locations of LPB subpopulations projecting to SNR (violet) or VTA (magenta). Note that CeA-projecting LPB neurons are predominantly located in the lateral parabrachial nucleus - external part (LPBe) (MPB: medial parabrachial nucleus). **(d)** EPSC generated at −70 mV by light stimulation of dorsal horn inputs to a retrogradely-labeled LPB neuron projecting to SNR (red trace: sample response after bath application of 20 μM CNQX; n = 10 cells; left) and mean EPSC amplitudes generated by light stimulation of dorsal horn inputs to LPB→SNR (n = 33 cells) and LPB→VTA neurons (n = 32 cells; right). Significance was calculated by means of unpaired t-test (q). Comparisons with no asterisk had $p > 0.05$ and were not considered significant. Data represent mean ± SEM.

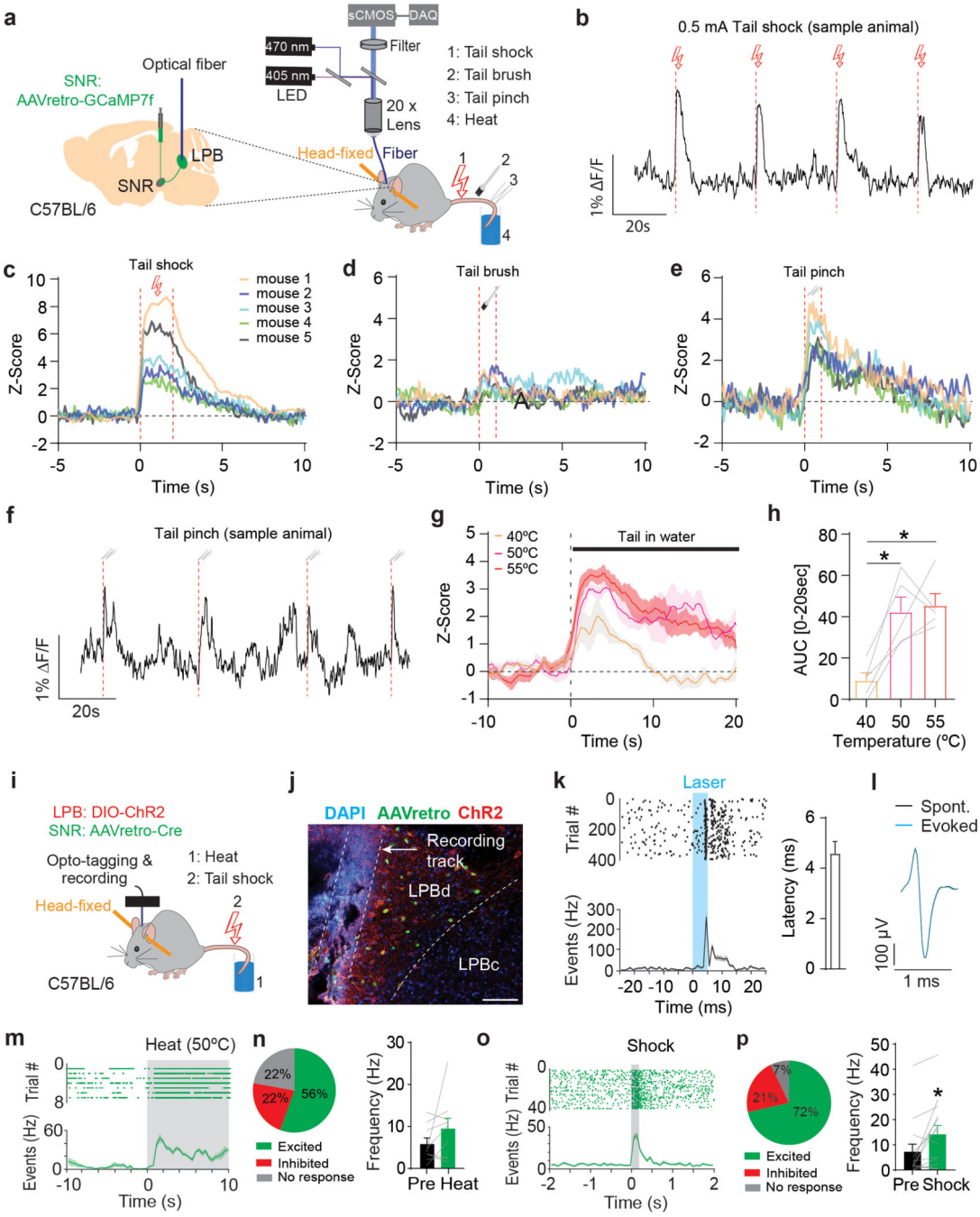

Fig. 3. LPB→SNR neurons represent diverse painful stimuli.

(a) Experimental design. **(b)** Response from LPB→SNR neurons to tail shock (red dashed lines; scale bars 0.5 mA/2 s). **(c-e)** Z score averages for LPB→SNR fluorescence in response to (c) tail shock, (d) tail brush, and (e) tail pinch for all animals (n = 8 trials per stimuli; n = 5 mice). **(f)** Sample response from LPB→SNR neurons to tail pinch (red dashed lines). **(g)** Z score averages for LPB→SNR fluorescence in response to heat exposure at 40°C (orange), 50°C (purple), or 55°C (magenta). Shading represents SEM (n = 3 trials per temperature level; n = 5 mice). **(h)** Significantly greater GCaMP7f response

from LPB→SNR neurons in response to heat exposure at 50°C and 55°C compared to 40°C (n = 3 trials per stimuli; n = 5 mice). **(i)** Experimental design. Activity of opto-tagged LPB neurons was recorded in response to heat (50°C, 10 sec) and tail shock (0.5 mA, 50 or 200 ms), n = 6 mice. **(j)** Location of optrode, AAVretro-Cre-eGFP (green) and ChR2 (red) in LPB (scale bar 100 μm). **(k)** Left: Raster plot showing latency of light-evoked spikes relative to light pulses (5 ms, blue; top) and corresponding spike firing frequency (bottom). Right: Mean response latency to laser stimulation for ChR2-tagged LPB→SNR neurons (n = 17 cells). **(l)** Sample waveform for evoked and spontaneous firing. **(m)** Sample of spike raster plot (top) and spontaneous firing frequency before and after (shaded) heat exposure (50°C, 10 sec) from an opto-tagged LPB→SNR neuron. **(n)** Left: Proportion of LPB→SNR neurons with significant increase (green), significant decrease (red) or no significant change (grey) in firing in response to heat (n = 9 cells). Right: Mean firing frequency of LPB→SNR neurons pre and post heat (n = 9 cells). **(o,p)** Same as in (m,n) but for electrical shock (n = 14 cells). Significance was calculated by means of one-way RM ANOVA with Tukey's post-hoc test (h) or paired t-test (n,p). * $p < 0.05$. Comparisons with no asterisk had $p > 0.05$ and were not considered significant. Data represent mean ± SEM.

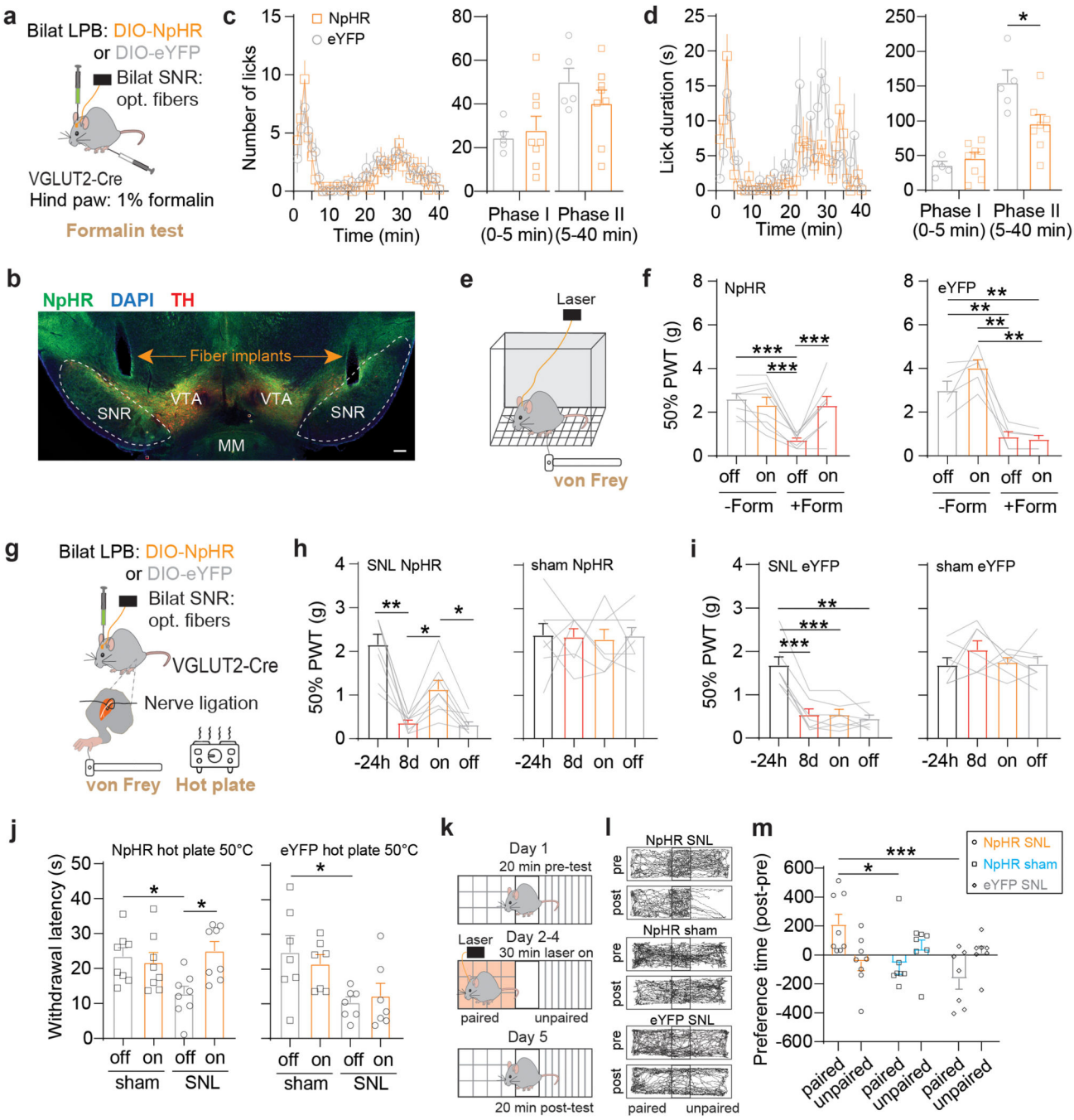

Fig. 4. Inhibition of LPB→SNR reduces behavioral responses to pain.

(a) Experimental design. **(b)** Implant locations (scale bar 200 μm). **(c)** Number of licks in response to formalin injection in NpHR (orange; n = 8) and eYFP (grey; n = 5) mice while exposing LPB_{VGLUT2} terminals in SNR to 589 nm light (left). Mean number of licks during phase I and phase II of formalin test for NpHR (orange) and eYFP (grey) mice. **(d)** Same as in (c) but for analysis of lick duration. **(e)** von Frey test. (**f**) Mean 50% paw withdrawal threshold (PWT) before formalin (-form) and after formalin (+form) injection for with (on) or without (off) 589 nm light for NpHR (left, n = 8) and eYFP (right; n =

5) mice. **(g)** Experimental design. **(h,i)** Mean 50% PWT measured 24 hours before and 8 days after SNL (left) or sham (right) surgery for (h) NpHR- and (i) eYFP-expressing mice. 'On' shows mean 50% PWT during 589 nm light exposure (SNL: NpHR: n = 8 mice, eYFP: n = 7 mice; sham: NpHR: n = 8 mice, eYFP: n = 7 mice). **(j)** Mean withdrawal latency during hot plate test at 50°C, 8 days after sham or SNL surgeries with (on) or without (off) 589 nm light exposure for NpHR- (left) and eYFP-expressing (right) mice (SNL: NpHR: n = 8, eYFP: n = 7; sham: NpHR: n = 8, eYFP: n = 7). **(k)** Experimental design. **(l)** Trajectories of sample NpHR SNL NpHR (top), NpHR sham (middle) and eYFP SNL (bottom) animals. Pre-tests were performed 8 days after SNL or sham surgeries. **(m)** NpHR SNL mice show significant increase in preference time for the side of the chamber paired with light stimulation compared to NpHR sham and eYFP SNL mice (NpHR SNL: n = 8; NpHR sham: n = 7; eYFP SNL: n = 7). Significance was calculated by means of two-way ANOVA with Holm-Sidak's post-hoc test (f,j,m), one-way RM ANOVA with Tukey's post-hoc test (h,i) or unpaired t-test (c,d). * $p < 0.05$, ** $p < 0.01$, *** $p < 0.001$. Data represent mean ± SEM.

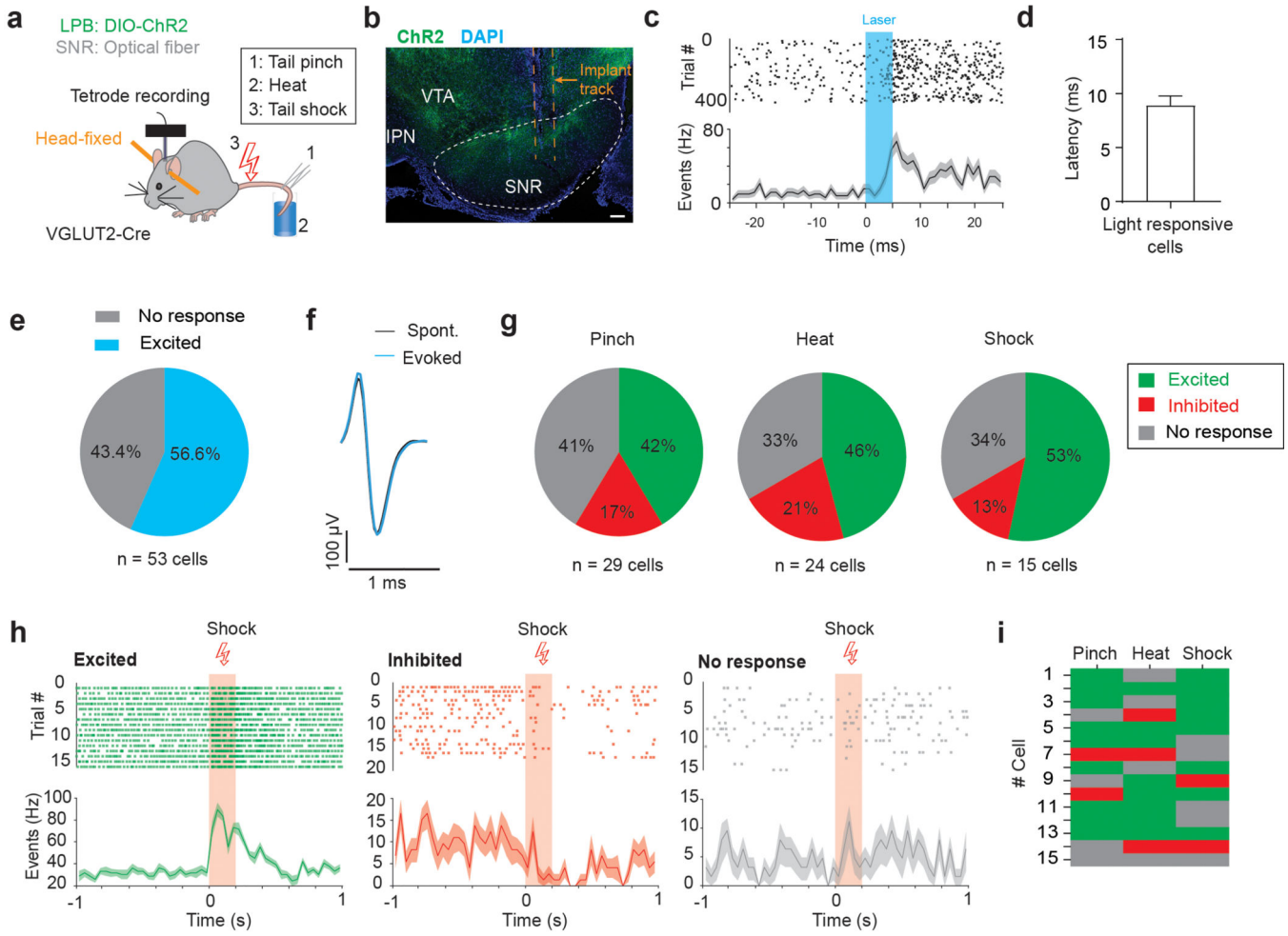

Fig. 5. LPB targeted SNR neurons are excited by noxious stimuli.

(a) Schematic showing unilateral targeting of AAV-DIO-ChR2 to LPB and placement of an optrode in the SNR of VGLUT2-Cre mice. Activity from SNR neurons was recorded in response to optogenetic stimulation of LPB inputs, tail pinch, heat (50°C, 10 sec) and electrical tail shock (0.5 mA, 200 ms; n = 5 mice). **(b)** Coronal section showing LPB_{VGLUT2} terminals expressing ChR2 (green) and location of optrode in lateral SNR (DAPI: blue; IPN: interpeduncular nucleus; VTA: ventral tegmental area; scale bar 100 µm). **(c)** Spike raster plot showing individual spikes in response to 5 ms laser pulse with each row representing individual trials (top) and the corresponding spike firing frequency (bottom). **(d)** Mean response latency to laser stimulation for LPB-targeted SNR neurons (n = 29 cells). **(e)** Proportion of SNR neurons that significantly increased firing in response to light stimulation of LPB inputs. **(f)** Samples of evoked and spontaneous action potential waveforms. **(g)** Proportion of LPB-targeted SNR neurons (i.e., SNR cells that showed significantly increased firing in response to light stimulation of LPB inputs) that were excited (green), inhibited (red) or did not respond (grey) following tail pinch, heat, or electrical shock (n = 15–29 cells from n = 5 mice). **(h)** Samples of spontaneous spike raster plots (top) and spontaneous firing frequencies (bottom) for LPB-targeted SNR neurons that were excited (left), inhibited (middle) or did not respond (right) to tail shock. **(i)** Responses

of LPB-targeted SNR neurons that were exposed to all three noxious stimuli (n = 15 cells). Data represent mean ± SEM.

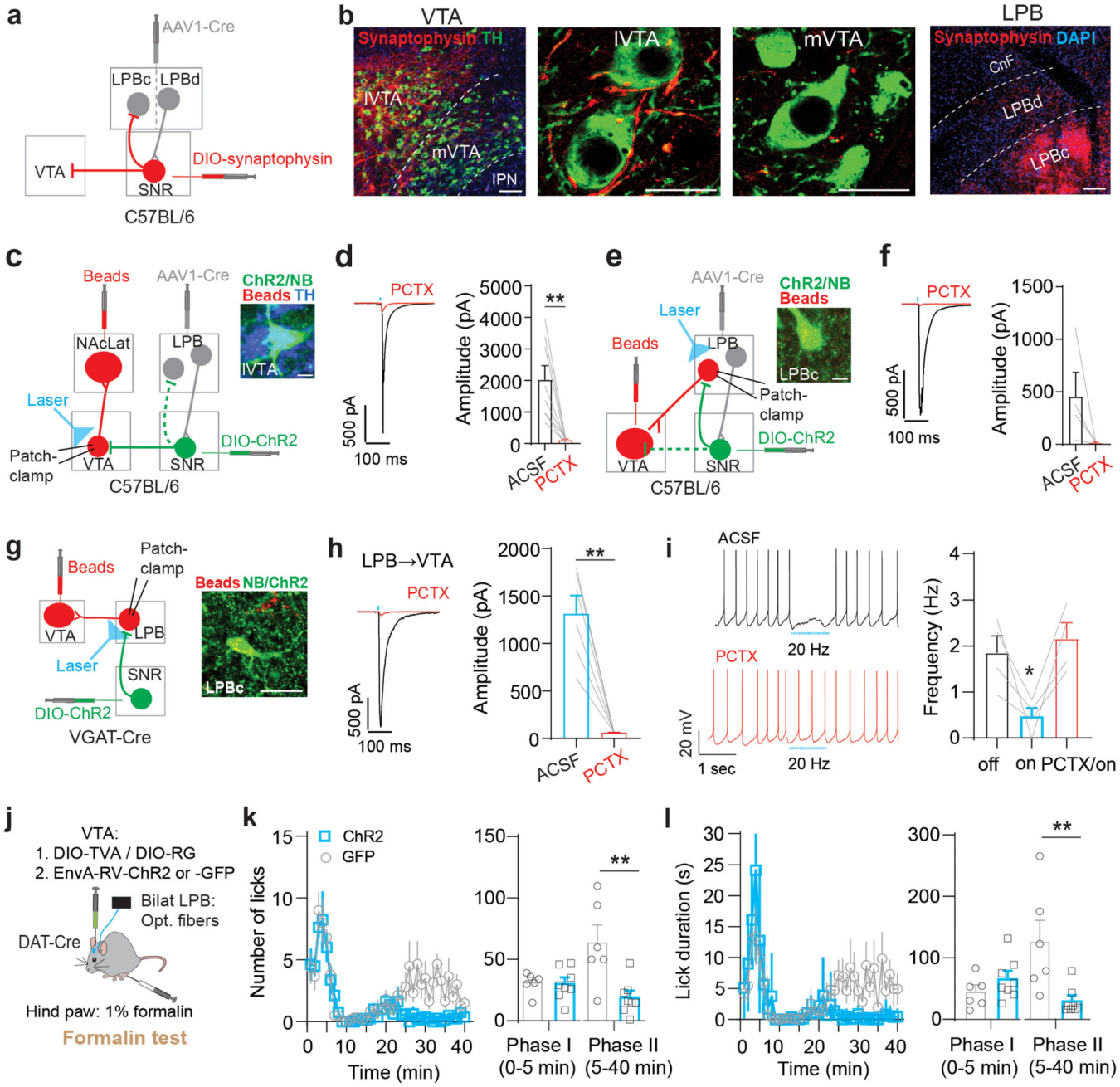

Fig. 6. LPB-targeted SNR neurons innervate VTA DA neurons directly and indirectly

(a) Experimental design. (b) Synaptophysin-expressing (red) terminals in lateral VTA (lVTA) and LPBc (scale bars 50 μm). (c) Experimental design. Inset: Neurobiotin (NB)-filled (green), TH-immunopositive (blue), retrogradely labeled (red) cell in lVTA (scale bar 10 μm). (d) Left: Light-evoked IPSC from NAcLat-projecting DA neuron (red trace: 100 μM picrotoxin (PCTX; scale bars 500 pA/100 ms). Right: Mean IPSC amplitudes recorded in NAcLat-projecting DA neurons before and after PCTX application (n = 8 cells). (e) Experimental design. Inset: Neurobiotin (NB)-filled (green), retrogradely labeled (red) LPBc cell (scale bar 10 μm). (f) Left: Light-evoked IPSC from LPB→VTA neuron

(red trace: 100 μM PCTX; scale bars 500 pA/100 ms). Right: Mean IPSC amplitudes recorded in LPB→VTA neurons before and after PCTX application (n = 4 cells). (g) Left: Experimental design. Right: Neurobiotin (NB)-filled (green), retrogradely labeled (red) LPBc cell (scale bar 50 μm). (h) Left: Sample IPSC generated at −70 mV by light stimulation of SNR_{VGAT} inputs to LPB→VTA neuron (red trace: 100 μM PCTX; scale bars 500 pA/100 ms). Right: Mean IPSC amplitudes before and after PCTX application (n = 6 cells). (i) Left: Spontaneous firing from LPB→VTA neuron before (top) and after (bottom) PCTX application in response to 20 Hz light stimulation of SNR_{VGAT} inputs (scale bars 20 mV/1 sec). Right: SNR_{VGAT} stimulation significantly reduces firing before but not after PCTX application in LPB→VTA neurons (n = 4 cells). (j) Experimental design. (k) Left: Number of licks in response to formalin injection in ChR2- (blue; n = 8) and GFP-expressing (grey; n = 6) mice while stimulating LPB→VTA DA neurons with 20 Hz blue light. Right: Mean number of licks during phase I and phase II of the formalin test for ChR2- (blue) and eYFP-expressing (grey) mice. (l) Same as in (k) but for analysis of lick duration. Significance was calculated by means of paired t-test (d,f,h), unpaired t-test (k,l) and one-way RM ANOVA with Tukey's post-hoc test (i). * $p < 0.05$, ** $p < 0.01$. Data represent mean ± SEM.

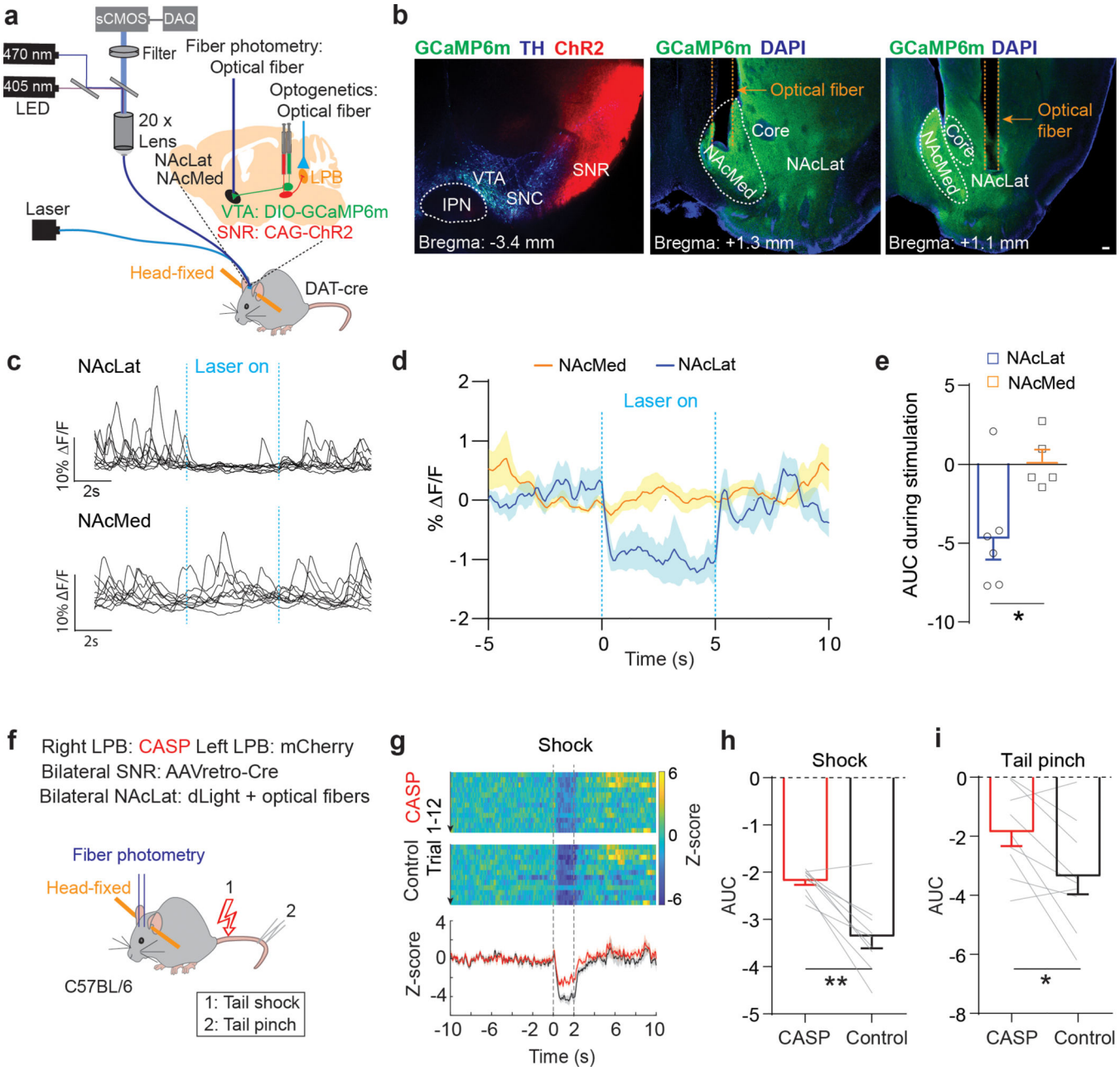

Fig. 7. LPB contributes to pain-induced inhibition of DA release *in vivo*.

(a) Schematic of viral targeting of ChR2 to lateral SNR and GCaMP6m to the VTA of DAT-Cre mice. Optogenetic stimulation of SNR terminals in the LPB and fiber photometry recordings of VTA DA terminals in NAc medial shell (NAcMed) or lateral shell (NAcLat). **(b)** Left: Coronal brain slice image showing ChR2 (red) expression in lateral SNR and GCaMP6m (green) expression in VTA DA neurons (TH: blue, SNC: substantia nigra pars compacta, IPN: interpeduncular nucleus). Middle: Coronal brain slice image showing optical fiber for fiber photometry recordings in NAcMed (DAPI: blue). Right: Coronal brain slice image showing optical fiber for fiber photometry recordings in NAcLat (scale bar 100 μm). **(c)** Sample GCaMP6m responses from VTA DA terminals in NAcLat (top)

and NAcMed (bottom) in response to 20 Hz optogenetic stimulation of SNR terminals in the LPB. **(d)** Comparison of mean GCaMP6m responses for recordings in NAcMed (red) and NAcLat (blue) in response to 20 Hz optogenetic stimulation of SNR terminals in the LPB. Shading represents SEM (n = 20–24 trials; NAcLat: n = 6 mice; NAcMed: n = 5 mice). **(e)** Comparison of mean AUC in NAcMed (orange) and NAcLat (blue) during optogenetic stimulation. **(f)** Schematic of experimental design showing bilateral targeting of AAVretro-Cre to SNR, unilateral targeting of AAV-DIO-Caspase 3 (CASP) to right LPB and control (AAV-DIO-mCherry) to left LPB of C57BL/6 mice. dLight1.2 and optical fibers were targeted bilaterally to NAcLat of the same animals (n = 9 mice). DA transients were recorded following electrical shock and tail pinch. **(g)** Top: Representative heat maps for NAcLat DA release from respective hemispheres as CASP and control vector expression in response to electrical shock. Bottom: Corresponding Z score averages (CASP: red, control: black). **(h,i)** Mean AUCs during shock (h) or tail pinch (i) for CASP and control sides. Significance was calculated by means of unpaired t-test (e) or paired t-test (h,i). * $p < 0.05$, ** $p < 0.01$. Comparisons with no asterisk had $p > 0.05$ and were not considered significant. Data represent mean ± SEM.

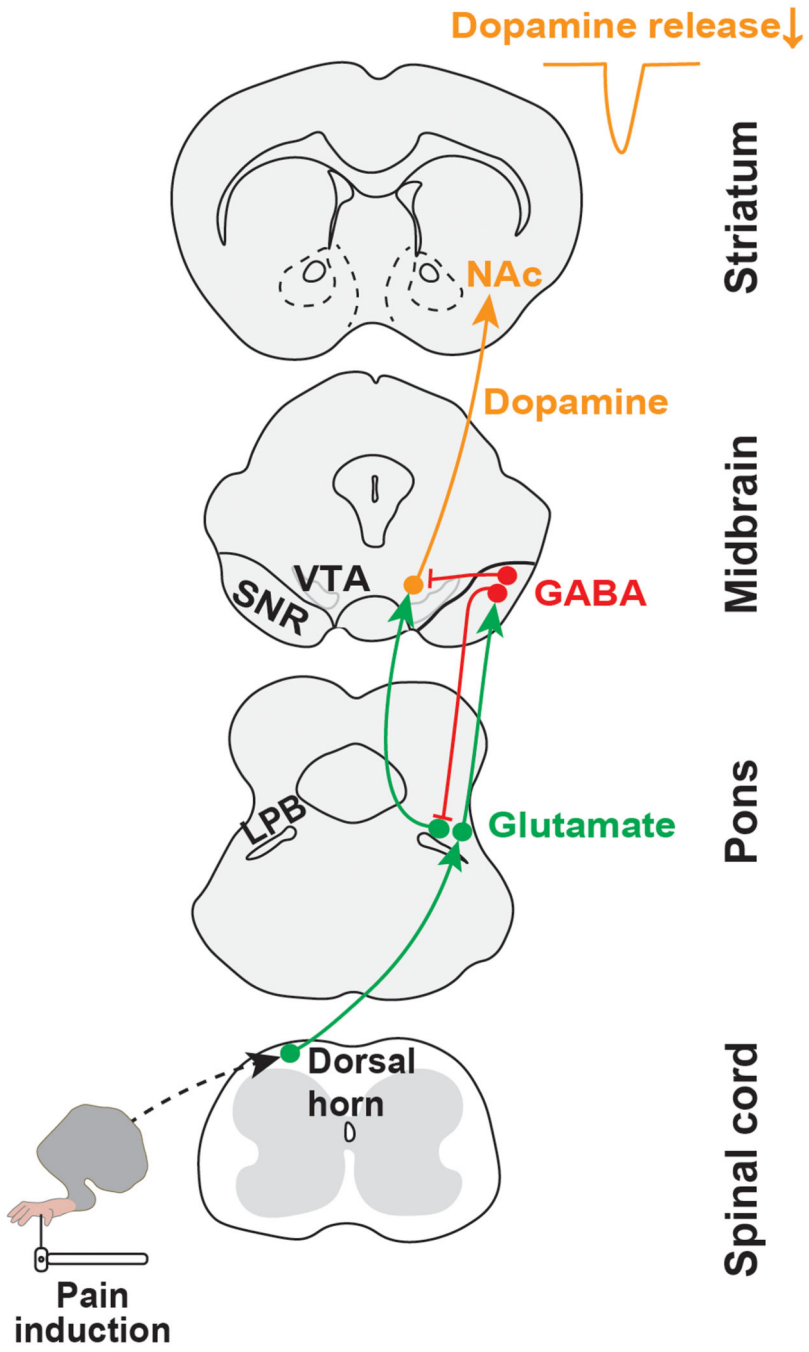

Fig. 8. Circuit model.

Schematic illustrating a neural circuit for conveying nociceptive input from the dorsal horn spinal cord to midbrain dopamine neurons projecting to NAcLat.